

# **M\_FCB User Manual**

## **Multi-frequency and multi-system FCB estimation software**

Caiya Yue

Email: [yuecaiya@lcu.edu.cn](mailto:yuecaiya@lcu.edu.cn)

## Contents

|   |    |
|---|----|
| 1. Introduction.....                                  | 3  |
| 2. Mathematical models .....                          | 3  |
| 2.1 Triple-frequency uncombined PPP .....             | 4  |
| 2.2 UWL-WL-NL FCB estimation .....                    | 8  |
| 2.3 Raw frequency FCB estimation .....                | 10 |
| 3. M_FCB software.....                                | 12 |
| 3.1 Dependencies .....                                | 13 |
| 3.2 Input file of raw frequency float ambiguity ..... | 14 |
| 3.3 Satellite altitude angle file.....                | 15 |
| 3.4 Cycle slip .....                                  | 16 |
| 3.5 FCB file.....                                     | 17 |
| 3.6 Control documents .....                           | 18 |
| 3.7 Directory and example of the software .....       | 19 |
| 4. How to Run the Software.....                       | 22 |
| 4.1 MATLAB version .....                              | 22 |
| 4.2 M_FCB software operation method.....              | 22 |
| 4.3 How to set whether the input file is read.....    | 23 |
| 5. Availability analysis of FCB .....                 | 24 |
| 5.1 UWL-WL-NL FCB .....                               | 24 |
| 5.2 Raw frequency FCB.....                            | 25 |
| 5.3 Validations of PPP AR with FCB correction.....    | 27 |
| 6. Acknowledgement and support.....                   | 29 |
| 7. References.....                                    | 29 |

## 1. Introduction

Precise point positioning (PPP) can achieve high-accuracy position information in any range of the world flexibly and efficiently without setting up base stations. Thus, PPP is considered as a new precision positioning mode following real-time kinematic (RTK) and network RTK positioning. With the continuous development of the global navigation satellite system (GNSS), multi-frequency and multi-system joint positioning has enhanced multi-level applications for PPP, such as the analysis of ionospheric refraction effects, real-time retrieval of precipitable water vapor, inversion of earthquakes and crustal deformation, unmanned driving in the urban environment and integrity monitoring. Although the PPP technique can bring great advantages, whether the ambiguity on the carrier phase observations can be resolved rapidly and accurately has been a key issue limiting its further application. The key to accurately and quickly fixing float ambiguity is to obtain high-precision and highly reliable fractional cycle bias (FCB). Some research institutions such as Centre National d'Etudes Spatiales (CNES), Center for Orbit Determination in Europe (CODE), GNSS Research Center at Wuhan University (WHU), and the School of Geodesy and Geomatics (SGG) at Wuhan University have released FCB products or integer recovered-clock (IRC) products to users for PPP AR. However, the above-mentioned FCB products can only be used with corresponding precise orbit and clock products, and it is difficult for users to fully understand the FCB calculation process and make improvements to it. Li et al. (2021) developed an open-sourced GREAT-UPD software for FCB estimation. This software can freely generate extra-wide-lane (EWL), wide-lane (WL), and narrow-lane (NL) FCBs for GPS, GLONASS, Galileo and BDS-2 satellites. Different from GREAT-UDP software, a MATLAB-based software for multi-GNSS FCB estimation (M\_FCB) was developed in this study. M\_FCB can not only estimate the FCB of GPS, BDS-2 and Galileo, but also can estimate BDS-3 satellites FCB. In the M-FCB software, we first calculate the float ambiguity on the raw frequency, and then develop two FCB estimation methods based on these float ambiguities, namely UWL-WL-NL FCB estimation and raw frequency FCB estimation. The UWL-WL-NL FCB estimation strategy in this software is different from that in GREAT-UDP software. We form UWL, WL, and NL combinations based on the raw frequency float ambiguity, while GREAT-UDP software is based on the Hatch-Melbourne-Wübbena combination (Hatch 1982; Melbourne 1985; Wübbena 1985).

## 2. Mathematical models

This section first introduces the triple-frequency uncombined PPP function model, and the detailed expression of the raw frequency float ambiguity is provided. then describes in detail two types of FCB estimation method.

## 2.1 Triple-frequency uncombined PPP

The basic model for the original multi-frequency GPS carrier phase and pseudo-range observations from receiver  $r$  to satellite  $s$  in units of length is:

$$\begin{cases} P_{r,j}^{s,G} = \rho_r^{s,G} + c \cdot (dt_r^G - dt^{s,G}) + M_r^{s,G} \cdot T_r^{s,G} + \gamma_j^G \cdot I_{r,1}^{s,G} + \\ \quad c \cdot (b_{r,j}^{s,G} - b_j^{s,G}) + \varepsilon_{r,j}^{s,G} \\ L_{r,j}^{s,G} = \lambda_j^G \varphi_{r,j}^{s,G} \\ \quad = \rho_r^{s,G} + c \cdot (dt_r^G - dt^{s,G}) + M_r^{s,G} \cdot T_r^{s,G} - \gamma_j^G \cdot I_{r,1}^{s,G} + \\ \quad \lambda_j^{s,G} (N_{r,j}^{s,G} + B_{r,j}^{s,G} + \partial B_{r,j}^{s,G} - B_j^{s,G} - \partial B_j^{s,G}) + e_{r,j}^{s,G} \end{cases} \quad (1)$$

To facilitate the derivation of subsequent formulas, the following expressions are defined:

$$\begin{cases} \alpha_{mn}^G = \frac{(f_m^{s,G})^2}{(f_m^{s,G})^2 - (f_n^{s,G})^2} \\ \beta_{mn}^G = -\frac{(f_n^{s,G})^2}{(f_m^{s,G})^2 - (f_n^{s,G})^2} \\ \text{DCB}_{P_m P_n}^{s,G} = b_m^{s,G} - b_n^{s,G} \\ \text{DCB}_{r, P_m P_n}^{s,G} = b_{r,m}^{s,G} - b_{r,n}^{s,G} \\ b_{IF_{mn}}^{s,G} = \alpha_{mn}^G \cdot b_m^{s,G} - \beta_{mn}^G \cdot b_n^{s,G} \\ b_{r, IF_{mn}}^{s,G} = \alpha_{mn}^G \cdot b_{r,m}^{s,G} - \beta_{mn}^G \cdot b_{r,n}^{s,G} \\ \partial \text{UPD}_{P_m P_n}^{s,G} = \partial B_m^{s,G} - \partial B_n^{s,G} \\ \partial \text{UPD}_{r, P_m P_n}^G = \partial B_{r,m}^G - \partial B_{r,n}^G \\ \partial B_{IF_{mn}}^{s,G} = \alpha_{mn}^G \cdot \partial B_m^{s,G} - \beta_{mn}^G \cdot \partial B_n^{s,G} \\ \partial B_{r, IF_{mn}}^G = \alpha_{mn}^G \cdot \partial B_{r,m}^G - \beta_{mn}^G \cdot \partial B_{r,n}^G \end{cases} \quad (2)$$

where superscript  $G$  denotes a satellite system;  $P_{r,j}^{s,G}$  and  $L_{r,j}^{s,G}$  denote the measured code and carrier phase, respectively;  $\rho_r^{s,G}$  is the geometric distance;  $c$  is the speed of light;  $dt_r^G$  and  $dt^{s,G}$  are the clock offsets of the receiver and satellite, respectively;  $M_r^{s,G}$  is the wet mapping function;  $T_r^{s,G}$  is the zenith wet delay;  $\gamma_j^G = (f_1^G / f_j^G)^2$  is the frequency-dependent multiplier factor, which is independent of the satellite pseudorandom noise code;  $I_{r,1}^{s,G}$  is the line-of-sight ionospheric delay on the frequency  $f_1^G$ ;  $\lambda_j^{s,G}$  is the carrier wavelength on the frequency  $f_j^G$ ;  $N_{r,j}^{s,G}$  is the integer phase ambiguity on the frequency  $f_j^G$ ;  $B_{r,j}^{s,G}$  and  $B_j^{s,G}$  are the time-invariance parts of the

frequency-dependent receiver and satellite uncalibrated phase delay (UPD), respectively;  $\partial B_{r,j}^{s,G}$  and  $\partial B_j^{s,G}$  are the time-varying parts of the frequency-dependent receiver and satellite UPD, respectively;  $b_{r,j}^{s,G}$  is the code hardware delay (CHD) from the receiver antenna to the signal correlator in the receiver;  $b_j^{s,G}$  is the CHD from the satellite signal generator to the satellite antenna;  $\varepsilon_{r,j}^{s,G}$  and  $e_{r,j}^{s,G}$  are the pseudo-range measurement noise and carrier measurement noise, respectively;  $f_m^{s,G}$  is the signal frequency of the  $m_{th}$  band of the system  $G$ ;  $\alpha_{mn}^G$  and  $\beta_{mn}^G$  are the frequency-dependent factors, respectively;  $DCB_{P_m P_n}^{s,G}$  and  $DCB_{r,P_m P_n}^{s,G}$  are the frequency-dependent satellite and receiver differential code bias, respectively;  $b_{IF_{mn}}^{s,G}$  and  $b_{r,IF_{mn}}^{s,G}$  are the IF combination of the CHD of the satellite and receiver, respectively;  $\partial UPD_{P_m P_n}^{s,G}$  and  $\partial UPD_{r,P_m P_n}^G$  are the differences in the time-varying part of the UPD on the differential frequency carrier phase in the satellite and receiver, respectively;  $\partial B_{IF_{mn}}^{s,G}$  and  $\partial B_{r,IF_{mn}}^G$  are the time-varying parts of IF combination of the UPD in the satellite and receiver, respectively. Other error items, such as phase center offsets and variations, phase windup, relativistic effect and tide loading, were assumed to be precisely corrected with their corresponding models.

Precise satellite clock products are generated by using the combination of IF observations. The carrier phase hardware delay is considered relatively stable for 24 hours or for a period of time, estimated as a constant, ignoring the time-varying part  $\partial B_j^{s,G}$ . Therefore, the satellite clock offsets  $dt_{IF_{12}}^{s,G}$  absorbs the IF combination satellite's CHD  $b_{IF_{12}}^{s,G}$  and the time-varying part of IF combination satellite's UPD  $\partial B_{IF_{12}}^{s,G}$ .

$$dt_{IF_{12}}^{s,G} = c \cdot dt^{s,G} + b_{IF_{12}}^{s,G} + \partial B_{IF_{12}}^{s,G} \quad (3)$$

Equation (3) is substituted into Equation (1) and then linearized using Taylor's formula. Moving the known items to the left of the equation and merging the same parameter items above, the equations on each frequency can be written in detail in the following form.  
For pseudo-range observables:

$$\begin{cases} \tilde{p}_{r,1}^{s,G} = \mathbf{u}_r^s \cdot \mathbf{x} + c \cdot dt_r^G + \mathbf{M}_r^{s,G} \cdot T_r^{s,G} + \gamma_1^G \cdot I_{r,1}^{s,G} + \\ \quad \bar{b}_{r,1}^{s,G} + \partial B_{IF_{12}}^{s,G} + \varepsilon_{r,1}^{s,G} \\ \tilde{p}_{r,2}^{s,G} = \mathbf{u}_r^s \cdot \mathbf{x} + c \cdot dt_r^G + \mathbf{M}_r^{s,G} \cdot T_r^{s,G} + \gamma_2^G \cdot I_{r,1}^{s,G} + \\ \quad \bar{b}_{r,2}^{s,G} + \partial B_{IF_{12}}^{s,G} + \varepsilon_{r,2}^{s,G} \\ \tilde{p}_{r,3}^{s,G} = \mathbf{u}_r^s \cdot \mathbf{x} + c \cdot dt_r^G + \mathbf{M}_r^{s,G} \cdot T_r^{s,G} + \gamma_3^G \cdot I_{r,1}^{s,G} + \\ \quad \bar{b}_{r,3}^{s,G} + \partial B_{IF_{12}}^{s,G} + \varepsilon_{r,3}^{s,G} \end{cases} \quad (4)$$

with

$$\begin{cases} \tilde{p}_{r,1}^{s,G} = P_{r,j}^{s,G} - \rho_r^s + dt_{IF_{12}}^{s,G} + \beta_{12} \cdot \text{DCB}_{P_1 P_2}^{s,G} \\ \tilde{p}_{r,2}^{s,G} = P_{r,j}^{s,G} - \rho_r^s + dt_{IF_{12}}^{s,G} - \alpha_{12} \cdot \text{DCB}_{P_1 P_2}^{s,G} \\ \tilde{p}_{r,3}^{s,G} = P_{r,j}^{s,G} - \rho_r^s + dt_{IF_{12}}^{s,G} - \alpha_{12} \cdot \text{DCB}_{P_1 P_3}^{s,G} - \beta_{12} \cdot \text{DCB}_{P_2 P_3}^{s,G} \end{cases} \quad (5)$$

For carrier phase observables:

$$\begin{cases} \tilde{l}_{r,1}^{s,G} = \mathbf{u}_r^s \cdot \mathbf{x} + c \cdot dt_r^G + \mathbf{M}_r^{s,G} \cdot T_r^{s,G} - \gamma_1^G \cdot I_{r,1}^{s,G} + \\ \quad \lambda_1^{s,G} N_{r,1}^{s,G} + B_{r,1}^{s,G} - B_1^{s,G} + b_{IF_{12}}^{s,G} + \partial B_{r,1}^{s,G} - \beta_{12} \partial \text{UPD}_{P_1 P_2}^{s,G} + e_{r,1}^{s,G} \\ \tilde{l}_{r,2}^{s,G} = \mathbf{u}_r^s \cdot \mathbf{x} + c \cdot dt_r^G + \mathbf{M}_r^{s,G} \cdot T_r^{s,G} - \gamma_2^G \cdot I_{r,1}^{s,G} + \\ \quad \lambda_2^{s,G} N_{r,2}^{s,G} + B_{r,2}^{s,G} - B_2^{s,G} + b_{IF_{12}}^{s,G} + \partial B_{r,2}^{s,G} + \alpha_{12} \partial \text{UPD}_{P_1 P_2}^{s,G} + e_{r,2}^{s,G} \\ \tilde{l}_{r,3}^{s,G} = \mathbf{u}_r^s \cdot \mathbf{x} + c \cdot dt_r^G + \mathbf{M}_r^{s,G} \cdot T_r^{s,G} - \gamma_3^G \cdot I_{r,1}^{s,G} + \\ \quad \lambda_1^{s,G} N_{r,3}^{s,G} + B_{r,3}^{s,G} - B_3^{s,G} + b_{IF_{12}}^{s,G} + \partial B_{r,3}^{s,G} - \partial B_3^{s,G} + \partial B_{IF_{12}}^{s,G} + e_{r,3}^{s,G} \end{cases} \quad (6)$$

with

$$\begin{cases} \tilde{l}_{r,1}^{s,G} = L_{r,1}^{s,G} - \rho_r^s + dt_{IF_{12}}^{s,G} \\ \tilde{l}_{r,2}^{s,G} = L_{r,2}^{s,G} - \rho_r^s + dt_{IF_{12}}^{s,G} \\ \tilde{l}_{r,3}^{s,G} = L_{r,3}^{s,G} - \rho_r^s + dt_{IF_{12}}^{s,G} \end{cases} \quad (7)$$

where  $\mathbf{u}_r^s$  is the unit vector of the component from the receiver to the satellite;  $\mathbf{x}$  is the vector of the receiver position increments relative to the priori position. Similarly, the receiver clocks are expressed in a form similar to the satellite clock offsets:

$$dt_{r,IF_{12}}^G = c \cdot dt_r^G + b_{r,IF_{12}}^G + \partial B_{r,IF_{12}}^G \quad (8)$$

Equation (8) is substituted into (4) and (6) and merged the same parameter items. The pseudo-range and carrier phase observation equations can be expressed as follows:

$$\begin{cases} \tilde{p}_{r,1}^{s,G} = \mathbf{u}_r^s \cdot \mathbf{x} + dt_{r,IF_{12}}^G + \mathbf{M}_r^{s,G} \cdot \mathbf{T}_r^{s,G} + \tilde{I}_{r,1}^{s,G} + \tau_{r,1}^{s,G} + \varepsilon_{r,1}^{s,G} \\ \tilde{p}_{r,2}^{s,G} = \mathbf{u}_r^s \cdot \mathbf{x} + dt_{r,IF_{12}}^G + \mathbf{M}_r^{s,G} \cdot \mathbf{T}_r^{s,G} + \gamma_2^G \cdot \tilde{I}_{r,1}^{s,G} + \tau_{r,2}^{s,G} + \varepsilon_{r,2}^{s,G} \\ \tilde{p}_{r,3}^{s,G} = \mathbf{u}_r^s \cdot \mathbf{x} + dt_{r,IF_{12}}^G + \mathbf{M}_r^{s,G} \cdot \mathbf{T}_r^{s,G} + \gamma_3^G \cdot \tilde{I}_{r,1}^{s,G} + IFB_{r,C} + \tau_{r,3}^{s,G} + \varepsilon_{r,3}^{s,G} \end{cases} \quad (9)$$

$$\begin{cases} \tilde{l}_{r,1}^{s,G} = \mathbf{u}_r^s \cdot \mathbf{x} + dt_{r,IF_{12}}^G + \mathbf{M}_r^{s,G} \cdot \mathbf{T}_r^{s,G} - \tilde{I}_{r,1}^{s,G} + \lambda_1^{s,G} \tilde{N}_{r,1}^{s,G} + e_{r,1}^{s,G} \\ \tilde{l}_{r,2}^{s,G} = \mathbf{u}_r^s \cdot \mathbf{x} + dt_{r,IF_{12}}^G + \mathbf{M}_r^{s,G} \cdot \mathbf{T}_r^{s,G} - \gamma_2^G \cdot \tilde{I}_{r,1}^{s,G} + \lambda_2^{s,G} \tilde{N}_{r,2}^{s,G} + e_{r,2}^{s,G} \\ \tilde{l}_{r,3}^{s,G} = \mathbf{u}_r^s \cdot \mathbf{x} + dt_{r,IF_{12}}^G + \mathbf{M}_r^{s,G} \cdot \mathbf{T}_r^{s,G} - \gamma_3^G \cdot \tilde{I}_{r,1}^{s,G} + \lambda_1^{s,G} \tilde{N}_{r,3}^{s,G} + IFCB_r^{s,G} + e_{r,3}^{s,G} \end{cases} \quad (10)$$

with

$$\begin{cases} \tilde{I}_{r,1}^{s,G} = I_{r,1}^{s,G} - \beta_{12} \cdot DCB_{r,P_1P_2}^{s,G} + \beta_{12} \cdot (\partial UPD_{P_1P_2}^{s,G} + \partial UPD_{r,P_1P_2}^{s,G}) \\ \tau_{r,1}^{s,G} = 2 \cdot \beta_{12} \cdot (\partial B_2^{s,G} + \partial B_{r,2}^G) + (\alpha_{12} + \beta_{12}) \cdot (\partial B_1^{s,G} + \partial B_{r,1}^G) \\ \tau_{r,2}^{s,G} = (\beta_{12} - \alpha_{12}) \cdot (\partial B_2^{s,G} + \partial B_{r,2}^G) + 2 \cdot \alpha_{12} \cdot (\partial B_1^{s,G} + \partial B_{r,1}^G) \\ \tau_{r,3}^{s,G} = (\gamma_3 + 1) \cdot (\partial B_2^{s,G} + \partial B_{r,2}^G) - (\gamma_2 + \gamma_3) \cdot (\partial B_1^{s,G} + \partial B_{r,1}^G) \\ IFB_{r,C} = (\gamma_3 - 1) \cdot \beta_{12} \cdot DCB_{r,P_1P_2}^{s,G} + DCB_{r,P_1P_3}^{s,G} \\ \tilde{N}_{r,1}^{s,G} = N_{r,1}^{s,G} + (B_{r,1}^{s,G} - B_1^{s,G} + b_{IF_{12}}^{s,G} - b_{r,IF_{12}}^{s,G} - \beta_{12} \cdot DCB_{r,P_1P_2}^{s,G}) / \lambda_1^{s,G} \\ \tilde{N}_{r,2}^{s,G} = N_{r,2}^{s,G} + (B_{r,2}^{s,G} - B_2^{s,G} + b_{IF_{12}}^{s,G} - b_{r,IF_{12}}^{s,G} - \gamma_2 \cdot \beta_{12} \cdot DCB_{r,P_1P_2}^{s,G}) / \lambda_2^{s,G} \\ \tilde{N}_{r,3}^{s,G} = N_{r,3}^{s,G} + (B_{r,3}^{s,G} - B_3^{s,G} + b_{IF_{12}}^{s,G} - b_{r,IF_{12}}^{s,G} - \gamma_3 \cdot \beta_{12} \cdot DCB_{r,P_1P_2}^{s,G}) / \lambda_3^{s,G} \\ IFCB_r^{s,G} = (\alpha_{12} + \gamma_3 \cdot \beta_{12}) \cdot (\partial B_1^{s,G} \cdot \partial B_{r,1}^G) + \beta_{12} \cdot (1 - \gamma_3) \cdot (\partial B_2^{s,G} + \partial B_{r,2}^G) \\ \quad - (\partial B_3^{s,G} + \partial B_{r,3}^G) \end{cases} \quad (11)$$

In Equations (9) and (10), the recombination ionospheric delay,  $\tilde{I}_{r,1}^{s,G}$ , absorbs the receiver differential code bias, the satellite's  $\partial UPD_{P_1P_2}^{s,G}$  and the receiver's  $\partial UPD_{r,P_1P_2}^{s,G}$ ;  $\tau_{r,i}^{s,G}$  ( $i = 1, 2, 3$ ) absorbs the time-varying part of the UPD in the first and second frequency, and this hardware delay bias does not require additional correction or estimation for its small magnitude (approximately 2 cm) and relatively low weight for the pseudo-range observation.  $\tilde{N}_{r,i}^{s,G}$  ( $i = 1, 2, 3$ ) is an ambiguity at the corresponding frequency and absorbs the time-invariance part of the UPD, receiver differential code bias and the IF combination of the CHD in the receiver and satellite;  $IFB_{r,C}$  is the satellite-independent inter-frequency bias parameter and, as for the triple-frequency PPP, the hardware biases on the L5 pseudo-range cannot be completely absorbed into the ionospheric delay, which was lumped in with the differential code biases between the L1 and L2 pseudo-ranges.  $IFCB_r^{s,G}$  is the IFCB related to the satellite. It is worth noting that in formula (5), some studies did

not correct the DCB, so the DCB parameters here will be absorbed by the ionospheric delay parameters in formula (11).

## 2.2 UWL-WL-NL FCB estimation

Taking GPS as an example, according to formula (11), the float ambiguity of each raw frequency after triple-frequency uncombined PPP Kalman filtering can be expressed as:

$$\begin{cases} \tilde{N}_{r,1}^{s,G} = N_{r,1}^{s,G} + (B_{r,1}^{s,G} - B_1^{s,G} + b_{IF_{12}}^{s,G} - b_{r,IF_{12}}^{s,G} - \beta_{12}^G \cdot \text{DCB}_{r,P_1P_2}^{s,G}) / \lambda_1^{s,G} \\ \tilde{N}_{r,2}^{s,G} = N_{r,2}^{s,G} + (B_{r,2}^{s,G} - B_2^{s,G} + b_{IF_{12}}^{s,G} - b_{r,IF_{12}}^{s,G} - \gamma_2 \cdot \beta_{12}^G \cdot \text{DCB}_{r,P_1P_2}^{s,G}) / \lambda_2^{s,G} \\ \tilde{N}_{r,3}^{s,G} = N_{r,3}^{s,G} + (B_{r,3}^{s,G} - B_3^{s,G} + b_{IF_{12}}^{s,G} - b_{r,IF_{12}}^{s,G} - \gamma_3 \cdot \beta_{12}^G \cdot \text{DCB}_{r,P_1P_2}^{s,G}) / \lambda_3^{s,G} \end{cases} \quad (12)$$

where:

$$\begin{cases} \text{DCB}_{r,P_1P_2}^{s,G} = \bar{b}_{r,1}^G - \bar{b}_{r,2}^G \\ b_{IF_{12}}^{s,G} = \alpha_{12}^G \cdot \bar{b}_1^{s,G} - \beta_{12}^G \cdot \bar{b}_2^{s,G} \\ b_{r,IF_{12}}^G = \alpha_{12}^G \cdot \bar{b}_{r,1}^G - \beta_{12}^G \cdot \bar{b}_{r,2}^G \\ \alpha_{12}^G = f_1^2 / (f_1^2 - f_2^2) \\ \beta_{12}^G = -f_2^2 / (f_1^2 - f_2^2) \end{cases} \quad (13)$$

where  $\tilde{N}_{r,i}^{s,G}$  ( $i = 1, 2, 3$ ) is the floating-point ambiguity at the corresponding frequency, measured in weeks. Which absorbs the time-varying stable hardware delay in the carrier phase and the pseudorange hardware delay at the receiver and satellite ends, thereby losing the integer characteristics.  $B_{r,i}^{s,G}$  and  $B_i^{s,G}$  are the time-varying stable hardware delay components in the carrier phase at the receiver and satellite ends, respectively.  $b_{IF_{12}}^{s,G}$  and  $b_{r,IF_{12}}^{s,G}$  are the code hardware delays for ionospheric free combinations at the satellite and receiver ends, respectively.  $\text{DCB}_{r,P_1P_2}^{s,G}$  is the differential code deviation at the receiver end. The meanings of other parameters can refer to Section 3.1.:

In order to achieve integer ambiguity, UPD at the satellite and receiver ends needs to be separated from integer ambiguity. However, due to the linear correlation between UPD and integer ambiguity, it is difficult to directly separate the integer part and ambiguity of UPD, and only the fractional cycle bias (FCB) of UPD at the satellite and receiver ends can be separated. In some studies, UPD and FCB are not subdivided, and usually both UPD and FCB refer to phase decimal deviations. Therefore, formula (12) can be written as:

$$\begin{aligned} \tilde{N}_{r,j}^{s,G} &= N_{r,j}^{s,G} + (B_{r,j}^{s,G} - B_j^{s,G} + b_{IF_{12}}^{s,G} - b_{r,IF_{12}}^{s,G} - \gamma_j \cdot \beta_{12}^G \cdot \text{DCB}_{r,P_1P_2}^{s,G}) / \lambda_j^{s,G} \\ &= N_{r,j}^{s,G} + \text{FCB}_{j,r} - \text{FCB}_j^s \end{aligned} \quad (14)$$



where

$$\begin{cases} FCB_{j,r} = (B_{r,j}^{s,G} - b_{r,IF_{12}}^{s,G} - \gamma_j \cdot \beta_{12}^G \cdot DCB_{r,P_1P_2}^{s,G}) / \lambda_j^{s,G} \\ FCB_j^s = (B_j^{s,G} + b_{IF_{12}}^{s,G}) / \lambda_j^{s,G} \end{cases} \quad (15)$$

where  $FCB_j^s$  is the FCB correction value required for fixing the float ambiguity of PPP. Analysis shows that there is a difference in the form of differential code deviation between the satellite side FCB and the receiver side FCB. This is mainly related to the constraint method of ionospheric delay parameters in uncombined PPP. FCB at different frequencies is a linear combination of phase hardware delay at each frequency and specific pseudorange hardware delay at two frequencies. It is not only affected by phase hardware delay at corresponding frequency, but also by specific pseudorange hardware delay. It should be noted that the two specific frequencies refer to those used to form ionospheric free combinations for generating precise orbits and clock bias products.

According to formula (14), a linear combination of ultra-wide lane can be formed. For GPS, the float ambiguity at the L2 frequency and the L5 frequency is generally combined.

$$\begin{aligned} F_{uwl} &= round(\tilde{N}_{r,2}^{s,G} - \tilde{N}_{r,5}^{s,G}) = (FCB_{2,r} - FCB_{5,r}) - (FCB_2^s - FCB_5^s) \\ &= FCB_{uwl,r} - FCB_{uwl}^s \end{aligned} \quad (16)$$

In formula (16),  $F_{uwl}$  is the decimal part of the float ambiguity of the ultra-wide lane, which can be obtained by direct integration.  $round(\cdot)$  is the integer operator.  $FCB_{uwl,r}$  and  $FCB_{uwl}^s$  are the ultra-wide lane FCB at the receiver end and the satellite end, respectively. For formula (16), the legal equation is rank deficient, and the M\_FCB software sets the FCB of the most observed satellite to 0 for the receiver and satellite FCB solution.

For wide lane linear combination, the float ambiguity on L1 frequency and L2 frequency can be combined according to formula (14).

$$\begin{aligned} F_{wl} &= round(\tilde{N}_{r,1}^{s,G} - \tilde{N}_{r,2}^{s,G}) = (FCB_{1,r} - FCB_{2,r}) - (FCB_1^s - FCB_2^s) \\ &= FCB_{wl,r} - FCB_{wl}^s \end{aligned} \quad (17)$$

where  $F_{wl}$  is the decimal part of the float ambiguity of the wide lane, which can be obtained by direct integration.  $FCB_{wl,r}$  and  $FCB_{wl}^s$  are the wide lane FCB at the receiver end and the satellite end, respectively. When solving the formula (17), the same algorithm is adopted as in the ultra-wide lane strategy.

For the narrow lane FCB estimation, ionosphere free combination is formed for the float ambiguity of L1 frequency and L2 frequency, and it is written in the form of the sum of the integer wide lane ambiguity and the ambiguity of narrow lane float ambiguity, as shown in formula (18).

When the wide lane FCB is solved, the integer wide lane ambiguity can be calculated by using formula (17). The float ambiguity of the narrow lane can be calculated according to the combination of the wide lane ambiguity and ionosphere free combination ambiguity, such as formula (19). For formula (19), the FCB estimation algorithm with the ultra-wide lane and the wide lane can be used to obtain the narrow lane FCB at the satellite end and the receiver end.

$$\tilde{N}_{r,IF}^{s,G} = \alpha_{12}^G \tilde{N}_{r,1}^{s,G} + \beta_{12}^G \tilde{N}_{r,2}^{s,G} = \tilde{N}_{r,NL}^{s,G} + \frac{f_2}{f_1 - f_2} N_{r,WL}^{s,G} \quad (18)$$

$$\tilde{N}_{r,NL}^{s,G} = \tilde{N}_{r,IF}^{s,G} - \frac{f_2}{f_1 - f_2} N_{r,WL}^{s,G} = N_{r,NL}^{s,G} + FCB_{nl,r} - FCB_{nl}^s \quad (19)$$

$$F_{nl} = \text{round}(\tilde{N}_{r,NL}^{s,G}) = FCB_{nl,r} - FCB_{nl}^s \quad (20)$$

where  $F_{nl}$  is the decimal part of the float ambiguity of the narrow lane.  $FCB_{nl,r}$  and  $FCB_{nl}^s$  are the narrow lane FCB at the receiver end and satellite ends, respectively.

### 2.3 Raw frequency FCB estimation

It is difficult to directly estimate the FCB at the raw frequency due to the short original frequency wavelength and the high correlation between the float ambiguity and the ionospheric delay. It is usually necessary to combine each original frequency ambiguity linearly to get a combination of ambiguity with longer wavelength and weak correlation. Many studies have shown that the combination of ultra-wide lane (0 1-1) and wide lane (1-1 0) can more effectively achieve FCB solution and ambiguity fixation. In addition, Li et al. (2018) conducted LAMBDA reduction correlation analysis concluded that narrow lane (4-3 0) combination to effectively reduce the correlation between float ambiguity and ionospheric delay. Therefore, the following linear combination system of equations is established:

$$\begin{bmatrix} F_{1,r}^s \\ F_{2,r}^s \\ F_{3,r}^s \end{bmatrix} = \begin{bmatrix} 0 & 1 & -1 & 0 & -1 & 1 \\ 1 & -1 & 0 & -1 & 1 & 0 \\ 4 & -3 & 0 & -4 & 3 & 0 \end{bmatrix} \begin{bmatrix} FCB_{1,r} \\ FCB_{2,r} \\ FCB_{3,r} \\ FCB_1^s \\ FCB_2^s \\ FCB_3^s \end{bmatrix} \quad (21)$$

where  $F_{1,r}^s$ ,  $F_{2,r}^s$  and  $F_{3,r}^s$  respectively are the decimal parts of the linear combination of the raw float ambiguity. Users can directly estimate the FCB at the original frequency through the formula. For narrow lane combinations, users can define them in the control file according to their own needs.

To improve the stability and continuity of FCB estimates, a globally uniformly distributed GNSS observation network is usually used. Assuming that there are  $n$  stations track  $m$  satellites in the observation network, the linear combination value of undifferenced float ambiguity of the satellite corresponding to each station in the continuous arc can be combined to form a large observation system.

To facilitate the description, define the following formula:

$$R = \begin{bmatrix} 0 & 1 & -1 \\ 1 & -1 & 0 \\ 4 & -3 & 0 \end{bmatrix} \quad I_m = \begin{bmatrix} 1 \\ 1 \\ \vdots \\ 1 \end{bmatrix}_m \quad (22)$$

$$e_n = \begin{bmatrix} 1 & & & \\ & 1 & & \\ & & \ddots & \\ & & & 1 \end{bmatrix}_n \quad e_m = \begin{bmatrix} 1 & & & \\ & 1 & & \\ & & \ddots & \\ & & & 1 \end{bmatrix}_m \quad (23)$$

The receiver-side FCB design matrix  $B_i$  of a single station  $i$  can be expressed as:

$$B_i = R \otimes I_m \quad (24)$$

When there is  $n$  stations, the receiver-end FCB design matrix  $B_n$  can be expressed as:

$$B_{n \times m} = B_i \otimes e_n \quad (25)$$

The FCB design matrix of  $n$  stations and  $m$  satellites can be expressed as:

$$S_{m \times n} = -R \otimes e_m \otimes e_n \quad (26)$$

The overall design matrix in the corresponding translation system can be expressed as:

$$A_n^m = \text{com}(B_{n \times m}, S_{m \times n}) \quad (27)$$

The corresponding estimated parameter  $X_n^m$  and the float ambiguity decimal part  $F_n^m$  after linear combination can be expressed as:

$$X_n^m = \underbrace{[FCB_{1,r_1}, FCB_{2,r_1}, FCB_{3,r_1}, \dots, FCB_{1,r_n}, FCB_{2,r_n}, FCB_{3,r_n}]}_{\text{Receivers}} \underbrace{[FCB_1^{s_1}, FCB_2^{s_1}, FCB_3^{s_1}, \dots, FCB_1^{s_m}, FCB_2^{s_m}, FCB_3^{s_m}]}_{\text{Satellites}}^T$$

$$F_n^m = [F_{1,r_1}^{s_1}, F_{2,r_1}^{s_1}, F_{3,r_1}^{s_1}, \dots, F_{1,r_1}^{s_m}, F_{2,r_1}^{s_m}, F_{3,r_1}^{s_m}, \dots, F_{1,r_n}^{s_1}, F_{2,r_n}^{s_1}, F_{3,r_n}^{s_1}, \dots, F_{1,r_n}^{s_m}, F_{2,r_n}^{s_m}, F_{3,r_n}^{s_m}]^T \quad (28)$$

When determining the weight of raw frequency float ambiguity, the function related to the satellite altitude angle is used:

$$P(E) = \begin{cases} 1.0, & E \geq 30^\circ \\ 2\sin(E), & \text{otherwise} \end{cases} \quad (29)$$

Using the variance-covariance propagation law, the system of observation equations in the whole translation system can be expressed as:

$$F_n^m = A_n^m \cdot X_n^m, \quad Q_n^m \quad (30)$$

In the above formula,  $\otimes$  is the Kronecker product operation,  $\text{com}$  is the matrix splicing operation, and  $Q_n^m$  is obtained from the variance-covariance propagation law. Due to the linear correlation between the receiver FCB and the satellite FCB at each frequency in the equation, the rank loss of the equation system is 3. Therefore, in M\_FCB, the most observed satellite  $s$  is selected as the benchmark, and the satellite end FCB value of each frequency on this satellite is set to 0, namely:

$$\begin{cases} FCB_1^s = 0 \\ FCB_2^s = 0 \\ FCB_3^s = 0 \end{cases} \quad (31)$$

Both the UWL-WL-NL FCB estimation method and the raw frequency FCB estimation method, the M\_FCB software uses iterative least squares to estimate the FCB of other satellites relative to the reference star.

### 3. M\_FCB software

The M\_FCB software is a scientific, high-precision, multi-GNSS FCB estimation software. It is based on the MATLAB platform, and almost all of the code is self-programmed and fully open-sourced. Thus, it is easy for users to study the FCB estimation algorithms and processes and implement further development according to their purposes. M\_FCB consists of three main functional components: file input and preprocessing, UWL-WL-NL FCB estimation and raw-frequency FCB estimation. A detailed flowchart of solving FCB is presented in Figure 1.

**(1) File Input and Preprocessing.** The files required for M\_FCB mainly include raw-frequency float ambiguity, satellite elevation angle, cycle slip files and control files. We provide additional executable programs to generate these files. Users can also generate these files using their own multi-frequency multi-system PPP data processing software and then utilize M\_FCB to solve FCBs. Therefore, M\_FCB can be easily extended and applied to other software. The control file mainly contains information on solving parameter settings, such as satellite system type, satellite cut-off elevation angle and solving time. After reading the input file, the program implements data preprocessing according to the control file, mainly including arc segment division, data screening and arc segment merging.

**(2) UWL-WL-NL FCB estimation.** Based on the control file information, UWL, WL and NL combinations are produced based on the raw-frequency float ambiguities. For the GPS satellite system, the inter-frequency clock bias (IFCB) is an important bias that affects the UWL FCB estimation. In general, when implementing multi-frequency PPP solving, IFCBs need to be acquired in advance and corrected directly based on the original observations. Our team has open-sourced the IFCB estimation software on GPS Toolbox (Yue et al., 2024). Users can directly use the software for IFCB generation and PPP solving. For NL FCB estimation, the ionosphere-free combination needs to be produced for the raw-frequency float ambiguity. After the WL ambiguity is fixed, the NL float ambiguity can be obtained to estimate NL FCBs. The solving process of UWL-WL-NL FCBs is to estimate the UWL FCB, then the WL FCB and finally the NL FCB.

**(3) Raw-frequency FCB estimation.** Raw-frequency float ambiguities are affected by ionospheric delay residuals and unmodeled errors and thus exhibit low accuracy. Therefore, when estimating the raw-frequency FCB, M\_FCB first performs a linear combination of the raw-frequency float ambiguities to obtain a combination with a long wavelength and a small ambiguity correlation. The coefficient matrix of combination can be read from the control file, and the default coefficient matrix in M\_FCB is based on Li et al. (2018). Users also can set the corresponding coefficient matrix in the control file according to their needs. According to the combined float ambiguity and the coefficient matrix, a system of equations was developed to estimate the three raw-frequency FCBs simultaneously.

Iterative least squares estimation is used for both UWL-WL-NL and raw-frequency FCB estimation. Regardless of which FCB estimation algorithm is used, the normal equation is rank-

deficient. Therefore, M\_FCB selects the most observed satellite as the benchmark for FCB estimation. The initial FCB value is calculated after the satellite benchmark is set. Then, the FCBs of all stations and satellites are solved by iterative least squares estimation. The estimated posteriori residuals larger than 0.25 cycles are down-weighted at each iteration until there are no more weights that can be down. Finally, the iteration is stopped to output the final FCB valuation.

In order to avoid confusion between our current M\_FCB software and the published M\_IFCB software, we provide the following explanation. Although both are deviations from GNSS precise positioning, they are completely different in terms of definition and correction methods. The main content of this manuscript is FCB, while our published manuscript focuses on IFCB. Because both of them are oriented towards multi-GNSS. Therefore, they are abbreviated as M\_FCB and M\_IFCB. Although their abbreviations are similar, they are two completely different objects. The function of FCB is to fix the ambiguity in PPP positioning. However, the role of IFCB is to correct systematic deviations in carrier phase in PPP observation models.

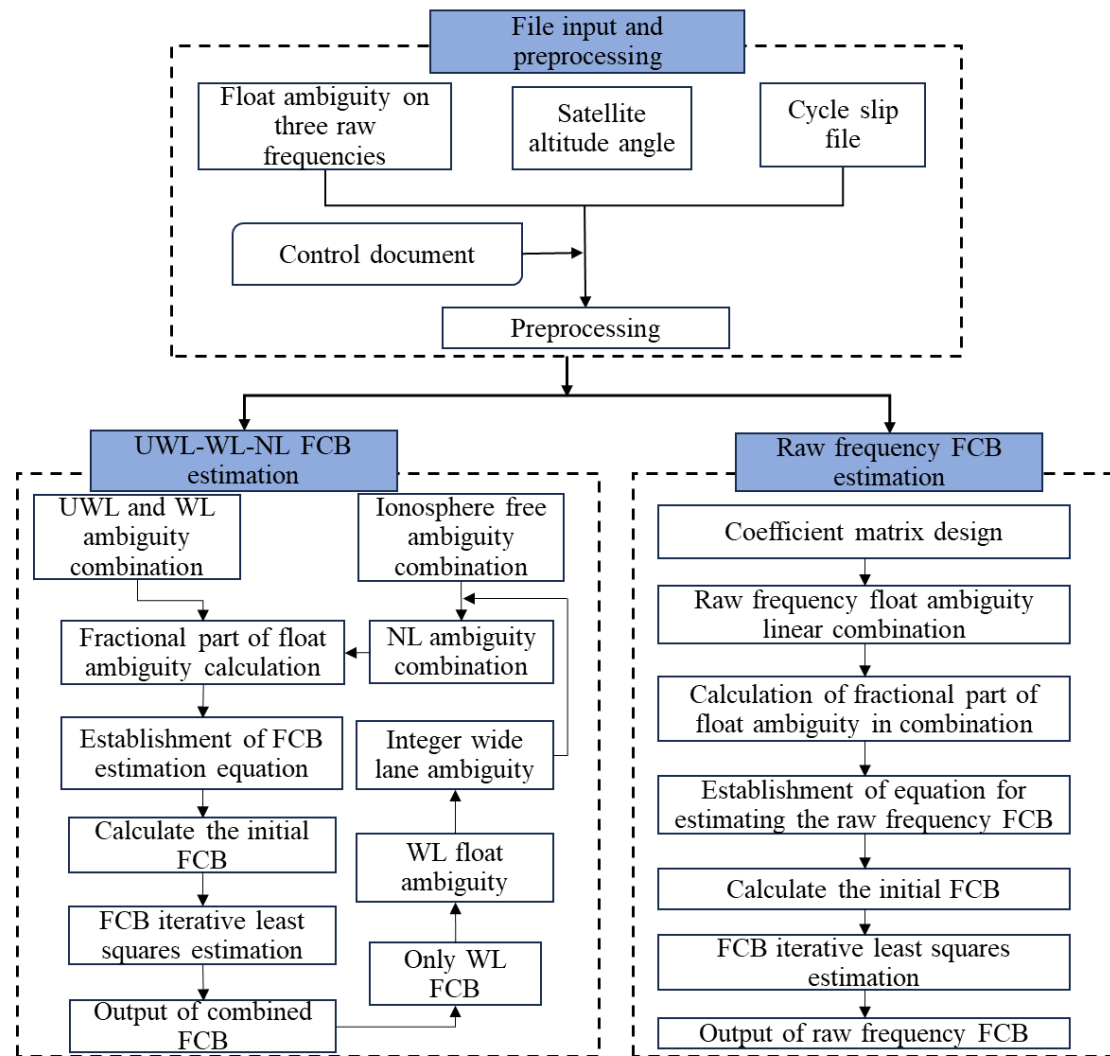


**Fig. 1** The flowchart of FCB estimation

### 3.1 Dependencies

The M\_FCB software is packaged as a MATLAB toolbox. The version used for software development is MATLAB 2016a.

### 3.2 Input file of raw frequency float ambiguity

M\_FCB can solve the FCBs of UWL, WL, and NL, as well as the FCBs of three raw frequencies. Therefore, there are also three input files for the raw frequency float ambiguity. The raw frequency float ambiguity file records the float ambiguity after Kalman filtering, and its specific expression is shown in formula (11). For the file format, the first eight columns record the time, from column 1 to column 8 are the year, month, day, hour, minute, second, GPS week, and seconds within a week, and from column 9 onwards, the float ambiguity for each satellite is recorded. The number of columns for float ambiguity values for GPS, BDS, and Galileo are 32, 60, and 40, respectively. The data in the green box in Figures 2~4 represents that the satellite can be observed and successfully calculated during the current epoch, while the number “9999.0000” in the red box represents that the station did not track the satellite during the current epoch or was not successfully calculated during the current epoch. Because the float ambiguity file can be easily output by PPP or other GNSS data processing software, the float ambiguity file is directly read in the M\_FCB estimation module, which also indicates that this software can be easily extended and applied to other software. The float ambiguity file format on the three frequencies is the same, only the file name and recorded content are different.

| ABP000MDG_R_20230400000_01D_30S_MO.rnx.amb1 |      |    |    |    |    |    |      |           |           |       |       |           |        |           |           |
|---|------|----|----|----|----|----|------|-----------|-----------|-------|-------|-----------|--------|-----------|-----------|
| 1   | 2023 | 02 | 09 | 00 | 00 | 00 | 2248 | 345600.00 | 99999.000 | 2.697 | 2.065 | 99999.000 | 10.291 | 99999.000 | 99999.000 |
| 2   | 2023 | 02 | 09 | 00 | 00 | 30 | 2248 | 345630.00 | 99999.000 | 2.248 | 1.976 | 99999.000 | 10.033 | 99999.000 | 99999.000 |
| 3   | 2023 | 02 | 09 | 00 | 01 | 00 | 2248 | 345660.00 | 99999.000 | 2.824 | 2.551 | 99999.000 | 10.224 | 99999.000 | 99999.000 |
| 4   | 2023 | 02 | 09 | 00 | 01 | 30 | 2248 | 345690.00 | 99999.000 | 2.756 | 2.526 | 99999.000 | 10.138 | 99999.000 | 99999.000 |
| 5   | 2023 | 02 | 09 | 00 | 02 | 00 | 2248 | 345720.00 | 99999.000 | 2.674 | 2.401 | 99999.000 | 10.005 | 99999.000 | 99999.000 |
| 6   | 2023 | 02 | 09 | 00 | 02 | 30 | 2248 | 345750.00 | 99999.000 | 2.830 | 2.525 | 99999.000 | 10.050 | 99999.000 | 99999.000 |
| 7   | 2023 | 02 | 09 | 00 | 03 | 00 | 2248 | 345780.00 | 99999.000 | 2.896 | 2.570 | 99999.000 | 10.092 | 99999.000 | 99999.000 |
| 8   | 2023 | 02 | 09 | 00 | 03 | 30 | 2248 | 345810.00 | 99999.000 | 2.857 | 2.471 | 99999.000 | 9.927  | 99999.000 | 99999.000 |
| 9   | 2023 | 02 | 09 | 00 | 04 | 00 | 2248 | 345840.00 | 99999.000 | 2.846 | 2.428 | 99999.000 | 9.889  | 99999.000 | 99999.000 |
| 10  | 2023 | 02 | 09 | 00 | 04 | 30 | 2248 | 345870.00 | 99999.000 | 2.803 | 2.354 | 99999.000 | 9.818  | 99999.000 | 99999.000 |
| 11  | 2023 | 02 | 09 | 00 | 05 | 00 | 2248 | 345900.00 | 99999.000 | 2.857 | 2.355 | 99999.000 | 9.743  | 99999.000 | 99999.000 |
| 12  | 2023 | 02 | 09 | 00 | 05 | 30 | 2248 | 345930.00 | 99999.000 | 2.901 | 2.336 | 99999.000 | 9.660  | 99999.000 | 99999.000 |
| 13  | 2023 | 02 | 09 | 00 | 06 | 00 | 2248 | 345960.00 | 99999.000 | 2.930 | 2.359 | 99999.000 | 9.622  | 99999.000 | 99999.000 |
| 14  | 2023 | 02 | 09 | 00 | 06 | 30 | 2248 | 345990.00 | 99999.000 | 2.943 | 2.357 | 99999.000 | 9.527  | 99999.000 | 99999.000 |
| 15  | 2023 | 02 | 09 | 00 | 07 | 00 | 2248 | 346020.00 | 99999.000 | 2.939 | 2.315 | 99999.000 | 9.431  | 99999.000 | 99999.000 |
| 16  | 2023 | 02 | 09 | 00 | 07 | 30 | 2248 | 346050.00 | 99999.000 | 3.017 | 2.329 | 99999.000 | 9.375  | 99999.000 | 99999.000 |
| 17  | 2023 | 02 | 09 | 00 | 08 | 00 | 2248 | 346080.00 | 99999.000 | 3.104 | 2.403 | 99999.000 | 9.388  | 99999.000 | 99999.000 |
| 18  | 2023 | 02 | 09 | 00 | 08 | 30 | 2248 | 346110.00 | 99999.000 | 3.168 | 2.452 | 99999.000 | 9.409  | 99999.000 | 99999.000 |
| 19  | 2023 | 02 | 09 | 00 | 09 | 00 | 2248 | 346140.00 | 99999.000 | 3.180 | 2.466 | 99999.000 | 9.418  | 99999.000 | 99999.000 |
| 20  | 2023 | 02 | 09 | 00 | 09 | 30 | 2248 | 346170.00 | 99999.000 | 3.236 | 2.525 | 99999.000 | 9.467  | 99999.000 | 99999.000 |
| 21  | 2023 | 02 | 09 | 00 | 10 | 00 | 2248 | 346200.00 | 99999.000 | 3.291 | 2.565 | 99999.000 | 9.489  | 99999.000 | 99999.000 |
| 22  | 2023 | 02 | 09 | 00 | 10 | 30 | 2248 | 346230.00 | 99999.000 | 3.321 | 2.556 | 99999.000 | 9.472  | 99999.000 | 99999.000 |
| 23  | 2023 | 02 | 09 | 00 | 11 | 00 | 2248 | 346260.00 | 99999.000 | 3.369 | 2.571 | 99999.000 | 9.467  | 99999.000 | 99999.000 |
| 24  | 2023 | 02 | 09 | 00 | 11 | 30 | 2248 | 346290.00 | 99999.000 | 3.415 | 2.602 | 99999.000 | 9.467  | 99999.000 | 99999.000 |
| 25  | 2023 | 02 | 09 | 00 | 12 | 00 | 2248 | 346320.00 | 99999.000 | 3.417 | 2.588 | 99999.000 | 9.429  | 99999.000 | 99999.000 |
| 26  | 2023 | 02 | 09 | 00 | 12 | 30 | 2248 | 346350.00 | 99999.000 | 3.417 | 2.572 | 99999.000 | 9.385  | 99999.000 | 99999.000 |
| 27  | 2023 | 02 | 09 | 00 | 13 | 00 | 2248 | 346380.00 | 99999.000 | 3.431 | 2.581 | 99999.000 | 9.353  | 99999.000 | 99999.000 |
| 28  | 2023 | 02 | 09 | 00 | 13 | 30 | 2248 | 346410.00 | 99999.000 | 3.452 | 2.620 | 99999.000 | 9.361  | 99999.000 | 99999.000 |
| 29  | 2023 | 02 | 09 | 00 | 14 | 00 | 2248 | 346440.00 | 99999.000 | 3.470 | 2.659 | 99999.000 | 9.380  | 99999.000 | 99999.000 |
| 30  | 2023 | 02 | 09 | 00 | 14 | 30 | 2248 | 346470.00 | 99999.000 | 3.495 | 2.688 | 99999.000 | 9.391  | 99999.000 | 99999.000 |
| 31  | 2023 | 02 | 09 | 00 | 15 | 00 | 2248 | 346500.00 | 99999.000 | 3.515 | 2.700 | 99999.000 | 9.395  | 99999.000 | 99999.000 |
| 32  | 2023 | 02 | 09 | 00 | 15 | 30 | 2248 | 346530.00 | 99999.000 | 3.533 | 2.716 | 99999.000 | 9.402  | 99999.000 | 99999.000 |

Fig. 2 Float ambiguity on L1 frequency



|   |      |    |    |    |    |    |      |           |           |       |        |           |        |           |           |
|---|------|----|----|----|----|----|------|-----------|-----------|-------|--------|-----------|--------|-----------|-----------|
| ABPO00MDG_R_20230400000_01D_30S_MO.rnx.amb2 |      |    |    |    |    |    |      |           |           |       |        |           |        |           |           |
| 1   | 2023 | 02 | 09 | 00 | 00 | 00 | 2248 | 345600.00 | 99999.000 | 2.658 | -0.753 | 99999.000 | 13.415 | 99999.000 | 99999.000 |
| 2   | 2023 | 02 | 09 | 00 | 00 | 30 | 2248 | 345630.00 | 99999.000 | 2.069 | -0.906 | 99999.000 | 13.054 | 99999.000 | 99999.000 |
| 3   | 2023 | 02 | 09 | 00 | 01 | 00 | 2248 | 345660.00 | 99999.000 | 2.795 | -0.155 | 99999.000 | 13.283 | 99999.000 | 99999.000 |
| 4   | 2023 | 02 | 09 | 00 | 01 | 30 | 2248 | 345690.00 | 99999.000 | 2.688 | -0.167 | 99999.000 | 13.150 | 99999.000 | 99999.000 |
| 5   | 2023 | 02 | 09 | 00 | 02 | 00 | 2248 | 345720.00 | 99999.000 | 2.581 | -0.347 | 99999.000 | 12.978 | 99999.000 | 99999.000 |
| 6   | 2023 | 02 | 09 | 00 | 02 | 30 | 2248 | 345750.00 | 99999.000 | 2.791 | -0.188 | 99999.000 | 13.056 | 99999.000 | 99999.000 |
| 7   | 2023 | 02 | 09 | 00 | 03 | 00 | 2248 | 345780.00 | 99999.000 | 2.871 | -0.150 | 99999.000 | 13.119 | 99999.000 | 99999.000 |
| 8   | 2023 | 02 | 09 | 00 | 03 | 30 | 2248 | 345810.00 | 99999.000 | 2.818 | -0.287 | 99999.000 | 12.901 | 99999.000 | 99999.000 |
| 9   | 2023 | 02 | 09 | 00 | 04 | 00 | 2248 | 345840.00 | 99999.000 | 2.807 | -0.351 | 99999.000 | 12.864 | 99999.000 | 99999.000 |
| 10  | 2023 | 02 | 09 | 00 | 04 | 30 | 2248 | 345870.00 | 99999.000 | 2.748 | -0.468 | 99999.000 | 12.769 | 99999.000 | 99999.000 |
| 11  | 2023 | 02 | 09 | 00 | 05 | 00 | 2248 | 345900.00 | 99999.000 | 2.818 | -0.479 | 99999.000 | 12.672 | 99999.000 | 99999.000 |
| 12  | 2023 | 02 | 09 | 00 | 05 | 30 | 2248 | 345930.00 | 99999.000 | 2.878 | -0.504 | 99999.000 | 12.564 | 99999.000 | 99999.000 |
| 13  | 2023 | 02 | 09 | 00 | 06 | 00 | 2248 | 345960.00 | 99999.000 | 2.918 | -0.471 | 99999.000 | 12.513 | 99999.000 | 99999.000 |
| 14  | 2023 | 02 | 09 | 00 | 06 | 30 | 2248 | 345990.00 | 99999.000 | 2.931 | -0.472 | 99999.000 | 12.384 | 99999.000 | 99999.000 |
| 15  | 2023 | 02 | 09 | 00 | 07 | 00 | 2248 | 346020.00 | 99999.000 | 2.921 | -0.532 | 99999.000 | 12.250 | 99999.000 | 99999.000 |
| 16  | 2023 | 02 | 09 | 00 | 07 | 30 | 2248 | 346050.00 | 99999.000 | 3.021 | -0.516 | 99999.000 | 12.175 | 99999.000 | 99999.000 |
| 17  | 2023 | 02 | 09 | 00 | 08 | 00 | 2248 | 346080.00 | 99999.000 | 3.136 | -0.422 | 99999.000 | 12.193 | 99999.000 | 99999.000 |
| 18  | 2023 | 02 | 09 | 00 | 08 | 30 | 2248 | 346110.00 | 99999.000 | 3.224 | -0.360 | 99999.000 | 12.227 | 99999.000 | 99999.000 |
| 19  | 2023 | 02 | 09 | 00 | 09 | 00 | 2248 | 346140.00 | 99999.000 | 3.240 | -0.339 | 99999.000 | 12.248 | 99999.000 | 99999.000 |
| 20  | 2023 | 02 | 09 | 00 | 09 | 30 | 2248 | 346170.00 | 99999.000 | 3.314 | -0.261 | 99999.000 | 12.327 | 99999.000 | 99999.000 |
| 21  | 2023 | 02 | 09 | 00 | 10 | 00 | 2248 | 346200.00 | 99999.000 | 3.387 | -0.208 | 99999.000 | 12.370 | 99999.000 | 99999.000 |
| 22  | 2023 | 02 | 09 | 00 | 10 | 30 | 2248 | 346230.00 | 99999.000 | 3.429 | -0.218 | 99999.000 | 12.360 | 99999.000 | 99999.000 |
| 23  | 2023 | 02 | 09 | 00 | 11 | 00 | 2248 | 346260.00 | 99999.000 | 3.493 | -0.196 | 99999.000 | 12.364 | 99999.000 | 99999.000 |
| 24  | 2023 | 02 | 09 | 00 | 11 | 30 | 2248 | 346290.00 | 99999.000 | 3.554 | -0.154 | 99999.000 | 12.371 | 99999.000 | 99999.000 |
| 25  | 2023 | 02 | 09 | 00 | 12 | 00 | 2248 | 346320.00 | 99999.000 | 3.558 | -0.172 | 99999.000 | 12.321 | 99999.000 | 99999.000 |
| 26  | 2023 | 02 | 09 | 00 | 12 | 30 | 2248 | 346350.00 | 99999.000 | 3.559 | -0.194 | 99999.000 | 12.260 | 99999.000 | 99999.000 |
| 27  | 2023 | 02 | 09 | 00 | 13 | 00 | 2248 | 346380.00 | 99999.000 | 3.578 | -0.182 | 99999.000 | 12.213 | 99999.000 | 99999.000 |
| 28  | 2023 | 02 | 09 | 00 | 13 | 30 | 2248 | 346410.00 | 99999.000 | 3.608 | -0.126 | 99999.000 | 12.219 | 99999.000 | 99999.000 |
| 29  | 2023 | 02 | 09 | 00 | 14 | 00 | 2248 | 346440.00 | 99999.000 | 3.630 | -0.073 | 99999.000 | 12.241 | 99999.000 | 99999.000 |
| 30  | 2023 | 02 | 09 | 00 | 14 | 30 | 2248 | 346470.00 | 99999.000 | 3.662 | -0.035 | 99999.000 | 12.252 | 99999.000 | 99999.000 |
| 31  | 2023 | 02 | 09 | 00 | 15 | 00 | 2248 | 346500.00 | 99999.000 | 3.687 | -0.019 | 99999.000 | 12.259 | 99999.000 | 99999.000 |

Fig. 3 Float ambiguity on L2 frequency

|   |      |    |    |    |    |    |      |           |           |        |       |           |        |           |           |           |
|---|------|----|----|----|----|----|------|-----------|-----------|--------|-------|-----------|--------|-----------|-----------|-----------|
| ABPO00MDG_R_20230400000_01D_30S_MO.rnx.amb3 |      |    |    |    |    |    |      |           |           |        |       |           |        |           |           |           |
| 1   | 2023 | 02 | 09 | 00 | 00 | 00 | 2248 | 345600.00 | 99999.000 | 10.377 | 0.407 | 99999.000 | 17.212 | 99999.000 | 99999.000 | 99999.000 |
| 2   | 2023 | 02 | 09 | 00 | 00 | 30 | 2248 | 345630.00 | 99999.000 | 9.801  | 0.260 | 99999.000 | 16.863 | 99999.000 | 99999.000 | 99999.000 |
| 3   | 2023 | 02 | 09 | 00 | 01 | 00 | 2248 | 345660.00 | 99999.000 | 10.512 | 0.991 | 99999.000 | 17.088 | 99999.000 | 99999.000 | 99999.000 |
| 4   | 2023 | 02 | 09 | 00 | 01 | 30 | 2248 | 345690.00 | 99999.000 | 10.411 | 0.977 | 99999.000 | 16.961 | 99999.000 | 99999.000 | 99999.000 |
| 5   | 2023 | 02 | 09 | 00 | 02 | 00 | 2248 | 345720.00 | 99999.000 | 10.306 | 0.803 | 99999.000 | 16.793 | 99999.000 | 99999.000 | 99999.000 |
| 6   | 2023 | 02 | 09 | 00 | 02 | 30 | 2248 | 345750.00 | 99999.000 | 10.510 | 0.958 | 99999.000 | 16.867 | 99999.000 | 99999.000 | 99999.000 |
| 7   | 2023 | 02 | 09 | 00 | 03 | 00 | 2248 | 345780.00 | 99999.000 | 10.588 | 0.997 | 99999.000 | 16.926 | 99999.000 | 99999.000 | 99999.000 |
| 8   | 2023 | 02 | 09 | 00 | 03 | 30 | 2248 | 345810.00 | 99999.000 | 10.535 | 0.864 | 99999.000 | 16.713 | 99999.000 | 99999.000 | 99999.000 |
| 9   | 2023 | 02 | 09 | 00 | 04 | 00 | 2248 | 345840.00 | 99999.000 | 10.524 | 0.802 | 99999.000 | 16.676 | 99999.000 | 99999.000 | 99999.000 |
| 10  | 2023 | 02 | 09 | 00 | 04 | 30 | 2248 | 345870.00 | 99999.000 | 10.468 | 0.690 | 99999.000 | 16.583 | 99999.000 | 99999.000 | 99999.000 |
| 11  | 2023 | 02 | 09 | 00 | 05 | 00 | 2248 | 345900.00 | 99999.000 | 10.536 | 0.680 | 99999.000 | 16.489 | 99999.000 | 99999.000 | 99999.000 |
| 12  | 2023 | 02 | 09 | 00 | 05 | 30 | 2248 | 345930.00 | 99999.000 | 10.594 | 0.655 | 99999.000 | 16.383 | 99999.000 | 99999.000 | 99999.000 |
| 13  | 2023 | 02 | 09 | 00 | 06 | 00 | 2248 | 345960.00 | 99999.000 | 10.633 | 0.687 | 99999.000 | 16.334 | 99999.000 | 99999.000 | 99999.000 |
| 14  | 2023 | 02 | 09 | 00 | 06 | 30 | 2248 | 345990.00 | 99999.000 | 10.646 | 0.686 | 99999.000 | 16.209 | 99999.000 | 99999.000 | 99999.000 |
| 15  | 2023 | 02 | 09 | 00 | 07 | 00 | 2248 | 346020.00 | 99999.000 | 10.636 | 0.627 | 99999.000 | 16.080 | 99999.000 | 99999.000 | 99999.000 |
| 16  | 2023 | 02 | 09 | 00 | 07 | 30 | 2248 | 346050.00 | 99999.000 | 10.734 | 0.642 | 99999.000 | 16.007 | 99999.000 | 99999.000 | 99999.000 |
| 17  | 2023 | 02 | 09 | 00 | 08 | 00 | 2248 | 346080.00 | 99999.000 | 10.846 | 0.734 | 99999.000 | 16.024 | 99999.000 | 99999.000 | 99999.000 |
| 18  | 2023 | 02 | 09 | 00 | 08 | 30 | 2248 | 346110.00 | 99999.000 | 10.932 | 0.794 | 99999.000 | 16.057 | 99999.000 | 99999.000 | 99999.000 |
| 19  | 2023 | 02 | 09 | 00 | 09 | 00 | 2248 | 346140.00 | 99999.000 | 10.947 | 0.815 | 99999.000 | 16.076 | 99999.000 | 99999.000 | 99999.000 |
| 20  | 2023 | 02 | 09 | 00 | 09 | 30 | 2248 | 346170.00 | 99999.000 | 11.018 | 0.890 | 99999.000 | 16.152 | 99999.000 | 99999.000 | 99999.000 |
| 21  | 2023 | 02 | 09 | 00 | 10 | 00 | 2248 | 346200.00 | 99999.000 | 11.089 | 0.942 | 99999.000 | 16.192 | 99999.000 | 99999.000 | 99999.000 |
| 22  | 2023 | 02 | 09 | 00 | 10 | 30 | 2248 | 346230.00 | 99999.000 | 11.130 | 0.932 | 99999.000 | 16.180 | 99999.000 | 99999.000 | 99999.000 |
| 23  | 2023 | 02 | 09 | 00 | 11 | 00 | 2248 | 346260.00 | 99999.000 | 11.192 | 0.954 | 99999.000 | 16.183 | 99999.000 | 99999.000 | 99999.000 |
| 24  | 2023 | 02 | 09 | 00 | 11 | 30 | 2248 | 346290.00 | 99999.000 | 11.251 | 0.995 | 99999.000 | 16.189 | 99999.000 | 99999.000 | 99999.000 |
| 25  | 2023 | 02 | 09 | 00 | 12 | 00 | 2248 | 346320.00 | 99999.000 | 11.255 | 0.977 | 99999.000 | 16.141 | 99999.000 | 99999.000 | 99999.000 |
| 26  | 2023 | 02 | 09 | 00 | 12 | 30 | 2248 | 346350.00 | 99999.000 | 11.256 | 0.956 | 99999.000 | 16.081 | 99999.000 | 99999.000 | 99999.000 |
| 27  | 2023 | 02 | 09 | 00 | 13 | 00 | 2248 | 346380.00 | 99999.000 | 11.275 | 0.967 | 99999.000 | 16.036 | 99999.000 | 99999.000 | 99999.000 |
| 28  | 2023 | 02 | 09 | 00 | 13 | 30 | 2248 | 346410.00 | 99999.000 | 11.303 | 1.021 | 99999.000 | 16.043 | 99999.000 | 99999.000 | 99999.000 |
| 29  | 2023 | 02 | 09 | 00 | 14 | 00 | 2248 | 346440.00 | 99999.000 | 11.325 | 1.073 | 99999.000 | 16.065 | 99999.000 | 99999.000 | 99999.000 |
| 30  | 2023 | 02 | 09 | 00 | 14 | 30 | 2248 | 346470.00 | 99999.000 | 11.356 | 1.109 | 99999.000 | 16.076 | 99999.000 | 99999.000 | 99999.000 |
| 31  | 2023 | 02 | 09 | 00 | 15 | 00 | 2248 | 346500.00 | 99999.000 | 11.380 | 1.125 | 99999.000 | 16.083 | 99999.000 | 99999.000 | 99999.000 |
| 32  | 2023 | 02 | 09 | 00 | 15 | 30 | 2248 | 346530.00 | 99999.000 | 11.400 | 1.146 | 99999.000 | 16.097 | 99999.000 | 99999.000 | 99999.000 |
| 33  | 2023 | 02 | 09 | 00 | 16 | 00 | 2248 | 346560.00 | 99999.000 | 11.416 | 1.152 | 99999.000 | 16.097 | 99999.000 | 99999.000 | 99999.000 |

Fig. 4 Float ambiguity on L5 frequency

### 3.3 Satellite altitude angle file

The satellite altitude angle file records satellite altitude angle data in degrees. The main purpose of this file is to provide the variance matrix during FCB least squares iterative estimation. The format of this file is completely consistent with the format of the DIF file.

| ABP000MDG_R_20230400000_01D_30S_MO.rnx.elev |      |    |    |    |    |    |      |           |           |        |        |           |        |           |           |
|---|------|----|----|----|----|----|------|-----------|-----------|--------|--------|-----------|--------|-----------|-----------|
| 1   | 2023 | 02 | 09 | 00 | 00 | 00 | 2248 | 345600.00 | 99999.000 | 26.002 | 26.499 | 99999.000 | 17.091 | 99999.000 | 99999.000 |
| 2   | 2023 | 02 | 09 | 00 | 00 | 30 | 2248 | 345630.00 | 99999.000 | 26.089 | 26.402 | 99999.000 | 16.965 | 99999.000 | 99999.000 |
| 3   | 2023 | 02 | 09 | 00 | 01 | 00 | 2248 | 345660.00 | 99999.000 | 26.176 | 26.305 | 99999.000 | 16.841 | 99999.000 | 99999.000 |
| 4   | 2023 | 02 | 09 | 00 | 01 | 30 | 2248 | 345690.00 | 99999.000 | 26.264 | 26.208 | 99999.000 | 16.716 | 99999.000 | 99999.000 |
| 5   | 2023 | 02 | 09 | 00 | 02 | 00 | 2248 | 345720.00 | 99999.000 | 26.352 | 26.111 | 99999.000 | 16.592 | 99999.000 | 99999.000 |
| 6   | 2023 | 02 | 09 | 00 | 02 | 30 | 2248 | 345750.00 | 99999.000 | 26.440 | 26.013 | 99999.000 | 16.469 | 99999.000 | 99999.000 |
| 7   | 2023 | 02 | 09 | 00 | 03 | 00 | 2248 | 345780.00 | 99999.000 | 26.529 | 25.916 | 99999.000 | 16.346 | 99999.000 | 99999.000 |
| 8   | 2023 | 02 | 09 | 00 | 03 | 30 | 2248 | 345810.00 | 99999.000 | 26.618 | 25.818 | 99999.000 | 16.223 | 99999.000 | 99999.000 |
| 9   | 2023 | 02 | 09 | 00 | 04 | 00 | 2248 | 345840.00 | 99999.000 | 26.708 | 25.720 | 99999.000 | 16.101 | 99999.000 | 99999.000 |
| 10  | 2023 | 02 | 09 | 00 | 04 | 30 | 2248 | 345870.00 | 99999.000 | 26.797 | 25.622 | 99999.000 | 15.979 | 99999.000 | 99999.000 |
| 11  | 2023 | 02 | 09 | 00 | 05 | 00 | 2248 | 345900.00 | 99999.000 | 26.887 | 25.524 | 99999.000 | 15.857 | 99999.000 | 99999.000 |
| 12  | 2023 | 02 | 09 | 00 | 05 | 30 | 2248 | 345930.00 | 99999.000 | 26.978 | 25.425 | 99999.000 | 15.736 | 99999.000 | 99999.000 |
| 13  | 2023 | 02 | 09 | 00 | 06 | 00 | 2248 | 345960.00 | 99999.000 | 27.068 | 25.326 | 99999.000 | 15.616 | 99999.000 | 99999.000 |
| 14  | 2023 | 02 | 09 | 00 | 06 | 30 | 2248 | 345990.00 | 99999.000 | 27.159 | 25.228 | 99999.000 | 15.495 | 99999.000 | 99999.000 |
| 15  | 2023 | 02 | 09 | 00 | 07 | 00 | 2248 | 346020.00 | 99999.000 | 27.250 | 25.129 | 99999.000 | 15.376 | 99999.000 | 99999.000 |
| 16  | 2023 | 02 | 09 | 00 | 07 | 30 | 2248 | 346050.00 | 99999.000 | 27.342 | 25.029 | 99999.000 | 15.256 | 99999.000 | 99999.000 |
| 17  | 2023 | 02 | 09 | 00 | 08 | 00 | 2248 | 346080.00 | 99999.000 | 27.434 | 24.930 | 99999.000 | 15.137 | 99999.000 | 99999.000 |
| 18  | 2023 | 02 | 09 | 00 | 08 | 30 | 2248 | 346110.00 | 99999.000 | 27.526 | 24.831 | 99999.000 | 15.019 | 99999.000 | 99999.000 |
| 19  | 2023 | 02 | 09 | 00 | 09 | 00 | 2248 | 346140.00 | 99999.000 | 27.619 | 24.731 | 99999.000 | 14.901 | 99999.000 | 99999.000 |
| 20  | 2023 | 02 | 09 | 00 | 09 | 30 | 2248 | 346170.00 | 99999.000 | 27.711 | 24.631 | 99999.000 | 14.783 | 99999.000 | 99999.000 |
| 21  | 2023 | 02 | 09 | 00 | 10 | 00 | 2248 | 346200.00 | 99999.000 | 27.805 | 24.532 | 99999.000 | 14.666 | 99999.000 | 99999.000 |
| 22  | 2023 | 02 | 09 | 00 | 10 | 30 | 2248 | 346230.00 | 99999.000 | 27.898 | 24.432 | 99999.000 | 14.549 | 99999.000 | 99999.000 |
| 23  | 2023 | 02 | 09 | 00 | 11 | 00 | 2248 | 346260.00 | 99999.000 | 27.992 | 24.332 | 99999.000 | 14.432 | 99999.000 | 99999.000 |
| 24  | 2023 | 02 | 09 | 00 | 11 | 30 | 2248 | 346290.00 | 99999.000 | 28.086 | 24.231 | 99999.000 | 14.316 | 99999.000 | 99999.000 |
| 25  | 2023 | 02 | 09 | 00 | 12 | 00 | 2248 | 346320.00 | 99999.000 | 28.181 | 24.131 | 99999.000 | 14.201 | 99999.000 | 99999.000 |
| 26  | 2023 | 02 | 09 | 00 | 12 | 30 | 2248 | 346350.00 | 99999.000 | 28.275 | 24.031 | 99999.000 | 14.086 | 99999.000 | 99999.000 |
| 27  | 2023 | 02 | 09 | 00 | 13 | 00 | 2248 | 346380.00 | 99999.000 | 28.371 | 23.930 | 99999.000 | 13.971 | 99999.000 | 99999.000 |
| 28  | 2023 | 02 | 09 | 00 | 13 | 30 | 2248 | 346410.00 | 99999.000 | 28.466 | 23.830 | 99999.000 | 13.857 | 99999.000 | 99999.000 |
| 29  | 2023 | 02 | 09 | 00 | 14 | 00 | 2248 | 346440.00 | 99999.000 | 28.562 | 23.729 | 99999.000 | 13.743 | 99999.000 | 99999.000 |
| 30  | 2023 | 02 | 09 | 00 | 14 | 30 | 2248 | 346470.00 | 99999.000 | 28.658 | 23.628 | 99999.000 | 13.629 | 99999.000 | 99999.000 |
| 31  | 2023 | 02 | 09 | 00 | 15 | 00 | 2248 | 346500.00 | 99999.000 | 28.754 | 23.527 | 99999.000 | 13.517 | 99999.000 | 99999.000 |
| 32  | 2023 | 02 | 09 | 00 | 15 | 30 | 2248 | 346530.00 | 99999.000 | 28.851 | 23.426 | 99999.000 | 13.404 | 99999.000 | 99999.000 |
| 33  | 2023 | 02 | 09 | 00 | 16 | 00 | 2248 | 346560.00 | 99999.000 | 28.948 | 23.325 | 99999.000 | 13.292 | 99999.000 | 99999.000 |
| 34  | 2023 | 02 | 09 | 00 | 16 | 30 | 2248 | 346590.00 | 99999.000 | 29.046 | 23.224 | 99999.000 | 13.180 | 99999.000 | 99999.000 |
| 35  | 2023 | 02 | 09 | 00 | 17 | 00 | 2248 | 346620.00 | 99999.000 | 29.144 | 23.123 | 99999.000 | 13.069 | 99999.000 | 99999.000 |

Fig. 5 Satellite altitude angle file

### 3.4 Cycle slip

The cycle slip file records whether the satellite has experienced a cycle slip in the current epoch. The first eight columns of this file represent time, which is consistent with the DIF file. Starting from the ninth column, record the flag indicating whether the satellite in the current epoch have undergone cycle slip. If the data is 0, it means that the satellite has not experienced a cycle slip in the current epoch. If it is 1 (as shown in the red box in the Figure 6), it means that the satellite has experienced a cycle slip.

| ABP000MDG_R_20230400000_01D_30S_MO.rnx.cslip |      |    |    |    |    |    |      |           |   |   |   |   |   |   |   |   |   |   |
|--|------|----|----|----|----|----|------|-----------|---|---|---|---|---|---|---|---|---|---|
| 1267   | 2023 | 02 | 09 | 10 | 33 | 00 | 2248 | 383580.00 | 0 | 0 | 0 | 0 | 0 | 0 | 0 | 0 | 0 | 0 |
| 1268   | 2023 | 02 | 09 | 10 | 33 | 30 | 2248 | 383610.00 | 0 | 0 | 0 | 0 | 0 | 0 | 0 | 0 | 0 | 0 |
| 1269   | 2023 | 02 | 09 | 10 | 34 | 00 | 2248 | 383640.00 | 0 | 0 | 0 | 0 | 0 | 0 | 0 | 0 | 0 | 0 |
| 1270   | 2023 | 02 | 09 | 10 | 34 | 30 | 2248 | 383670.00 | 0 | 0 | 0 | 0 | 0 | 0 | 0 | 0 | 0 | 0 |
| 1271   | 2023 | 02 | 09 | 10 | 35 | 00 | 2248 | 383700.00 | 0 | 0 | 0 | 0 | 0 | 0 | 0 | 0 | 0 | 0 |
| 1272   | 2023 | 02 | 09 | 10 | 35 | 30 | 2248 | 383730.00 | 0 | 0 | 0 | 0 | 0 | 0 | 0 | 0 | 0 | 0 |
| 1273   | 2023 | 02 | 09 | 10 | 36 | 00 | 2248 | 383760.00 | 0 | 0 | 0 | 0 | 0 | 0 | 0 | 0 | 0 | 0 |
| 1274   | 2023 | 02 | 09 | 10 | 36 | 30 | 2248 | 383790.00 | 0 | 0 | 0 | 0 | 0 | 0 | 0 | 0 | 0 | 0 |
| 1275   | 2023 | 02 | 09 | 10 | 37 | 00 | 2248 | 383820.00 | 0 | 0 | 0 | 0 | 0 | 0 | 0 | 0 | 0 | 0 |
| 1276   | 2023 | 02 | 09 | 10 | 37 | 30 | 2248 | 383850.00 | 0 | 0 | 0 | 0 | 0 | 0 | 0 | 0 | 0 | 0 |
| 1277   | 2023 | 02 | 09 | 10 | 38 | 00 | 2248 | 383880.00 | 0 | 0 | 0 | 0 | 0 | 0 | 0 | 0 | 0 | 0 |
| 1278   | 2023 | 02 | 09 | 10 | 38 | 30 | 2248 | 383910.00 | 0 | 0 | 0 | 0 | 0 | 0 | 0 | 0 | 0 | 0 |
| 1279   | 2023 | 02 | 09 | 10 | 39 | 00 | 2248 | 383940.00 | 0 | 0 | 0 | 0 | 0 | 0 | 0 | 0 | 0 | 0 |
| 1280   | 2023 | 02 | 09 | 10 | 39 | 30 | 2248 | 383970.00 | 0 | 0 | 0 | 0 | 0 | 0 | 0 | 0 | 0 | 0 |
| 1281   | 2023 | 02 | 09 | 10 | 40 | 00 | 2248 | 384000.00 | 0 | 0 | 0 | 0 | 0 | 0 | 0 | 0 | 0 | 0 |
| 1282   | 2023 | 02 | 09 | 10 | 40 | 30 | 2248 | 384030.00 | 0 | 0 | 0 | 0 | 0 | 0 | 0 | 0 | 0 | 0 |
| 1283   | 2023 | 02 | 09 | 10 | 41 | 00 | 2248 | 384060.00 | 0 | 0 | 0 | 0 | 0 | 0 | 0 | 0 | 0 | 0 |
| 1284   | 2023 | 02 | 09 | 10 | 41 | 30 | 2248 | 384090.00 | 0 | 0 | 0 | 0 | 0 | 0 | 0 | 0 | 0 | 0 |
| 1285   | 2023 | 02 | 09 | 10 | 42 | 00 | 2248 | 384120.00 | 0 | 0 | 0 | 0 | 0 | 0 | 0 | 0 | 0 | 0 |
| 1286   | 2023 | 02 | 09 | 10 | 42 | 30 | 2248 | 384150.00 | 0 | 0 | 0 | 0 | 0 | 0 | 0 | 0 | 0 | 0 |
| 1287   | 2023 | 02 | 09 | 10 | 43 | 00 | 2248 | 384180.00 | 0 | 0 | 0 | 0 | 0 | 0 | 0 | 0 | 0 | 1 |
| 1288   | 2023 | 02 | 09 | 10 | 43 | 30 | 2248 | 384210.00 | 0 | 0 | 0 | 0 | 0 | 0 | 0 | 0 | 0 | 1 |
| 1289   | 2023 | 02 | 09 | 10 | 44 | 00 | 2248 | 384240.00 | 0 | 0 | 0 | 0 | 0 | 0 | 0 | 0 | 0 | 1 |
| 1290   | 2023 | 02 | 09 | 10 | 44 | 30 | 2248 | 384270.00 | 0 | 0 | 0 | 0 | 0 | 0 | 0 | 0 | 0 | 1 |
| 1291   | 2023 | 02 | 09 | 10 | 45 | 00 | 2248 | 384300.00 | 0 | 0 | 0 | 0 | 0 | 0 | 0 | 0 | 0 | 1 |
| 1292   | 2023 | 02 | 09 | 10 | 45 | 30 | 2248 | 384330.00 | 0 | 0 | 0 | 0 | 0 | 0 | 0 | 0 | 0 | 1 |

Fig. 6 Cycle slip files



### 3.5 FCB file

The FCB file records the estimated FCB values for each satellite system. Because M\_FCB can not only estimate UWL-WL-NL FCB, but also estimate FCB at the original frequency. Therefore, these two types of files have differences in format. For UWL FCB and WL FCB, although the M\_FCB software defaults to estimating a value every 30 minutes, due to its good stability within a single day, users can use the average value of FCB calculated within a day to fix the corresponding ambiguity. For narrow lane FCB, the default value of the M\_FCB software is also estimated every 30 minutes. Users can set the FCB estimation duration in the control file to meet their needs.

Figure 7 shows the estimated UWL-WL-NL FCB result of each satellite at 00:00:00 on DOY 038 in the year 2023, using Galileo as an example. The sampling interval information can be found in the header file. The unit of FCB value is cycle. In the output FCB file, the first to third columns are UWL FCB, WL FCB, and NL FCB, respectively.

As shown in the red box in Figure 7, this satellite may not have been successfully resolved due to no data broadcast or poor quality. We directly assign the value of "999.99" to this type of satellite.

|    |                           |                   |          |                      |
|----|---------------------------|-------------------|----------|----------------------|
| 1  | 1.00                      | FCB DATA          | E        | VERSION / TYPE       |
| 2  | LUC                       |                   |          | RUN BY / DATE        |
| 3  | ****,                     |                   |          | ANALYSIS CENTER      |
| 4  | Email:yuecaiya@luc.edu.cn |                   |          | COMMENT              |
| 5  | GEC2C3 igs igs20.atx      |                   |          | SYS/EXT PROD APPLIED |
| 6  | 1                         |                   |          | # OF SOLN STA        |
| 7  | ****                      |                   |          | STA NAME LIST        |
| 8  | ****                      | UWL WL NL (cycle) |          | FCB type             |
| 9  | 30.0 min                  |                   |          | SAMPLING INTERVAL    |
| 10 | *2023_02_07 0 0 0         |                   |          |                      |
| 11 | E01                       | -0.0989           | 0.4863   | 0.0337               |
| 12 | E02                       | -0.1454           | -0.3153  | 0.0547               |
| 13 | E03                       | 0.0577            | 0.0959   | -0.0290              |
| 14 | E04                       | -0.2248           | 0.3035   | 0.0910               |
| 15 | E05                       | 0.0681            | 0.2020   | -0.0532              |
| 16 | E06                       | 999.9900          | 999.9900 | 999.9900             |
| 17 | E07                       | 0.0997            | 0.4715   | -0.0196              |
| 18 | E08                       | -0.2862           | 0.2209   | 0.1584               |
| 19 | E09                       | 0.0000            | 0.0000   | 0.0000               |
| 20 | E10                       | -0.0911           | 0.3774   | 0.0450               |
| 21 | E11                       | 0.1363            | 0.1212   | 0.4148               |
| 22 | E12                       | 999.9900          | 999.9900 | 999.9900             |
| 23 | E13                       | 999.9900          | 999.9900 | 999.9900             |
| 24 | E14                       | 999.9900          | 999.9900 | 999.9900             |
| 25 | E15                       | 999.9900          | 999.9900 | 999.9900             |
| 26 | E16                       | 999.9900          | 999.9900 | 999.9900             |
| 27 | E17                       | 999.9900          | 999.9900 | 999.9900             |
| 28 | E18                       | 999.9900          | 999.9900 | 999.9900             |
| 29 | E19                       | 999.9900          | 999.9900 | 999.9900             |
| 30 | E20                       | 999.9900          | 999.9900 | 999.9900             |
| 31 | E21                       | -0.0077           | 0.2772   | 0.0144               |
| 32 | E22                       | 999.9900          | 999.9900 | 999.9900             |
| 33 | E23                       | 999.9900          | 999.9900 | 999.9900             |
| 34 | E24                       | 999.9900          | 999.9900 | 999.9900             |

**Fig. 7** The result of estimated UWL-WL-NL FCB

Figure 8 shows the estimated raw frequency FCB results on DOY 038 in the year 2023. The sampling interval information can also be found in the file header. The unit of FCB value is also a

cycle. In the output FCB file, the first to third columns are the first frequency FCB (E1), the second frequency FCB (E5a), and the third frequency FCB (E5b), respectively. The first and second frequencies are used for IGS precise ephemeris estimation.

| cgs202338_raw_E.fcb |             |                  |           |                      |
|---------------------|-------------|------------------|-----------|----------------------|
| 1                   | 1.00        | FCB DATA         | E         | VERSION / TYPE       |
| 2                   | CGS         |                  |           | RUN BY / DATE        |
| 3                   | CASM,       |                  |           | ANALYSIS CENTER      |
| 4                   | Email:      |                  |           | COMMENT              |
| 5                   | GEC2C3      | igs              | igs14.atx | SYS/EXT PROD APPLIED |
| 6                   | 1           |                  |           | # OF SOLN STA        |
| 7                   | ****        |                  |           | STA NAME LIST        |
| 8                   | ****        | L1 L2 L3 (cycle) |           | FCB type             |
| 9                   | 30.0 min    |                  |           | SAMPLING INTERVAL    |
| 10                  | *2023_02_07 | 0 0 0            |           |                      |
| 11                  | E01         | 0.3663           | 0.4018    | -0.1655              |
| 12                  | E02         | -0.1302          | -0.1337   | 0.1908               |
| 13                  | E03         | -0.1393          | 0.5402    | 0.3971               |
| 14                  | E04         | 0.0813           | 0.2565    | 0.8057               |
| 15                  | E05         | -0.0381          | -0.2564   | -0.0443              |
| 16                  | E06         | 999.9900         | 999.9900  | 999.9900             |
| 17                  | E07         | -0.5991          | 0.0164    | -0.1728              |
| 18                  | E08         | -0.2710          | 0.7034    | -0.1477              |
| 19                  | E09         | 99999.9990       | 0.0000    | -0.0000              |
| 20                  | E10         | -0.2620          | -0.4624   | -0.6902              |
| 21                  | E11         | -0.1931          | 0.1165    | 0.2175               |
| 22                  | E12         | 999.9900         | 999.9900  | 999.9900             |
| 23                  | E13         | 999.9900         | 999.9900  | 999.9900             |
| 24                  | E14         | 999.9900         | 999.9900  | 999.9900             |
| 25                  | E15         | 999.9900         | 999.9900  | 999.9900             |
| 26                  | E16         | 999.9900         | 999.9900  | 999.9900             |
| 27                  | E17         | 999.9900         | 999.9900  | 999.9900             |
| 28                  | E18         | 999.9900         | 999.9900  | 999.9900             |
| 29                  | E19         | 999.9900         | 999.9900  | 999.9900             |
| 30                  | E20         | 999.9900         | 999.9900  | 999.9900             |
| 31                  | E21         | 0.0012           | -0.3521   | -0.4045              |
| 32                  | E22         | 999.9900         | 999.9900  | 999.9900             |
| 33                  | E23         | 999.9900         | 999.9900  | 999.9900             |
| 34                  | E24         | 999.9900         | 999.9900  | 999.9900             |
| 35                  | E25         | 999.9900         | 999.9900  | 999.9900             |
| 36                  | E26         | 0.0421           | -0.4993   | -0.0530              |
| 37                  | E27         | 0.0485           | 0.9291    | 0.7517               |

**Fig. 8** The result of estimated raw frequency FCB

### 3.6 Control documents

The control information of M\_FCB is all written in the "UD\_read\_configuration.m" script. This control script mainly includes three parts, namely the constant part, the important control strategy part, and the output part. The constant part mainly provides the frequency of each satellite system, while the output part mainly provides the output name and path of the FCB estimation file.

The important control strategy section contains rich control information about the use of FCB estimation, including satellite cut-off altitude angle setting, threshold setting, arc segment merging setting, and output sampling interval (as shown in Figure 9). In addition, options for UWL-WL-NL FCB estimation method and raw frequency FCB estimation method are also included in this section. Users can set according to their own needs. During the execution process, the first step of the M\_FCB is to read control file information.

```

%% Configuration option
cfg.elev=15; % satellite cut-off altitude angle (°)
cfg.inter=30; % raw data sampling interval (s)
cfg.span_t=30; % UPD/FCB output sampling interval (min)
cfg.com3='4 -3 0'; % NL combination coefficients for estimating raw frequency FCB/UPD
cfg.amb='amb1 amb2 amb3'; % floating ambiguity
cfg.plot_flag=1; % 0: not plotting; 1: plot FCB/UPD
cfg.upd_sitelst=1; % 0: Do not update station list; 1: update station list
cfg.amb_thr='0.15 0.2 0.25'; % median exclusion threshold for UWL, WL and NL
cfg.sigma='3.0 3.0 2.0'; % threshold of n times sigma for UWL, WL and NL
cfg.fix_amb='0.25 0.25 0.9'; % adjustment weight reduction threshold (cycle), fixed ambiguity threshold (cycle), adjustment weight reduction value
cfg.weight=1; % 0: equal-weighted; 1: STD weight calculation
cfg.original_upd=0; % 0: first epoch; 1: each epoch
cfg.cslip_thr=0.90; % Sort the stations based on the total number of cycle slips and retain stations within this rate
cfg.dir='data_dir';
cfg.yyyy=yyyy;
cfg.doy=doy;
cfg.FCB_M00=2; % 1: raw FCB 2: UWL-WL-NL FCB
cfg.NavSystem=NavSystem;
if(cfg.NavSystem==1); cfg.NPRN=32; end % number of satellites
if(cfg.NavSystem==2); cfg.NPRN=40; end
if(cfg.NavSystem==3); cfg.NPRN=60; end
if(cfg.NavSystem==4); cfg.NPRN=60; end
if(cfg.NavSystem==5);
    cfg.new_ban=2; % 1: B1C 2: B2a
end
%-----Arc segment merging control strategy-----
if(cfg.NavSystem==1); cfg.comb_time=90; end % minimum arc segment for merging (min)
if(cfg.NavSystem==2); cfg.comb_time=120; end
if(cfg.NavSystem==3); cfg.comb_time=120; end
if(cfg.NavSystem==4); cfg.comb_time=120; end
%-----Excluded satellites-----
if(cfg.NavSystem==1); cfg.rem_prn='00 00'; end
if(cfg.NavSystem==2); cfg.rem_prn='00 12 13 15 19 24 25'; end
if(cfg.NavSystem==3); cfg.rem_prn='00 00'; end
if(cfg.NavSystem==4); cfg.rem_prn='00 36 41 42'; end
cfg.comb_arc=30; % merge the data from the last 30 minutes as the ambiguity parameter
cfg.nprn_C2=16; % number of BDS-2 satellites
cfg.geo_flag=0; % 0: do not estimate GEO satellite; 1: estimate GEO satellite
cfg.ref_prn=0; % 0: max satellite 1: max site

```

Fig. 9 Control strategy section of M\_FCB software

### 3.7 Directory and example of the software

We provide a software package named "M\_FCB", which includes the "code" folder, "data" folder, "result" folder, "tools" folder, and user manual.






|   |                        |                |                             |
|---|------------------------|----------------|-----------------------------|
|  | code                   | 2024/8/2 13:17 | 文件夹                         |
|  | data                   | 2024/8/2 13:39 | 文件夹                         |
|  | result                 | 2024/8/2 13:22 | 文件夹                         |
|  | tools                  | 2024/8/2 13:21 | 文件夹                         |
|  | M_FCB user manual.docx | 2024/8/2 13:34 | Microsoft Word ... 2,508 KB |

Fig. 9 M\_FCB software package

**(1) Data:** In M\_FCB software, input data is placed in data, such as directory “2023038\_E”, which includes raw frequency float ambiguity files (with the suffix “.amb1”, “.amb2” and “.amb3”), satellite altitude angle files (with the suffix “.elev”), and cycle jump files (with the suffix “.cslip”). Users can set the corresponding format when generating these three types of files using their own software. For the convenience of users using M\_FCB, we provide tools for solving these three files (the directory of “Tools”) (as shown in Figure 10). For a detailed introduction to this tool, please refer to "readme.docx" under "Tools"

|  |                 |          |          |
|--|-----------------|----------|----------|
| ABPO00MDG_R_20230380000_01D_30S_MO.rnx.amb1  | 2024/7/24 19:26 | AMB1 文件  | 1,230 KB |
| ABPO00MDG_R_20230380000_01D_30S_MO.rnx.amb2  | 2024/7/24 19:26 | AMB2 文件  | 1,230 KB |
| ABPO00MDG_R_20230380000_01D_30S_MO.rnx.amb3  | 2024/7/24 19:26 | AMB3 文件  | 1,230 KB |
| ABPO00MDG_R_20230380000_01D_30S_MO.rnx.canc  | 2024/7/24 19:26 | CANC 文件  | 330 KB   |
| ABPO00MDG_R_20230380000_01D_30S_MO.rnx.cslip | 2024/7/24 19:26 | CSLIP 文件 | 555 KB   |
| ABPO00MDG_R_20230380000_01D_30S_MO.rnx.elev  | 2024/7/24 19:26 | ELEV 文件  | 1,230 KB |
| ABPO00MDG_R_20230380000_01D_30S_MO.rnx.pos   | 2024/7/24 19:26 | POS 文件   | 411 KB   |
| ACRG00GHA_R_20230380000_01D_30S_MO.rnx.amb1  | 2024/7/24 19:27 | AMB1 文件  | 1,230 KB |
| ACRG00GHA_R_20230380000_01D_30S_MO.rnx.amb2  | 2024/7/24 19:27 | AMB2 文件  | 1,230 KB |
| ACRG00GHA_R_20230380000_01D_30S_MO.rnx.amb3  | 2024/7/24 19:27 | AMB3 文件  | 1,230 KB |
| ACRG00GHA_R_20230380000_01D_30S_MO.rnx.canc  | 2024/7/24 19:27 | CANC 文件  | 330 KB   |
| ACRG00GHA_R_20230380000_01D_30S_MO.rnx.cslip | 2024/7/24 19:27 | CSLIP 文件 | 555 KB   |
| ACRG00GHA_R_20230380000_01D_30S_MO.rnx.elev  | 2024/7/24 19:27 | ELEV 文件  | 1,230 KB |
| ACRG00GHA_R_20230380000_01D_30S_MO.rnx.pos   | 2024/7/24 19:27 | POS 文件   | 411 KB   |

**Fig. 11** The directory of Tools for computer input files

**(2) Result:** The FCB estimation results and others process documents are included in this directory. The naming convention for output files is "result+S+yyyy+boy". Here, S represents the type of satellite system, with E for Galileo satellite system, G for GPS, C2 for BDS-2, and C3 for BDS-3. The name of the FCB estimation result given using the Galileo satellite system as an example is "result\_E\_2023038".

There are several files in this directory that are worth explaining in detail. The first one is "cgs2023038\_LC\_E.fcb". The final solution result of FCB is recorded here, as shown in Figure 7. The second file is "upd\_debug\_u\_2023038.txt", "upd\_debugw\_2023038.txt" or "upd\_debug\_n\_2023038.txt". It records the estimated number of iterations for each FCB and the proportion of residual errors less than 0.25 cycles and 0.15 cycles, respectively, as shown in Figures 11-13. In Figures 11-13, the third to last column, the second to last column, and the first to last column represent the proportion of iterations and posterior residuals less than 0.25 cycles and 0.15 cycles, respectively. Another important file is "sol\_rog.txt", which records the entire FCB calculation process.

|    |   |   |       |       |
|----|---|---|-------|-------|
| 1  | Numbers of iterations and fix rate of UWL FCB | 2 | 1.000 | 1.000 |
| 2  | Numbers of iterations and fix rate of UWL FCB | 2 | 1.000 | 1.000 |
| 3  | Numbers of iterations and fix rate of UWL FCB | 3 | 1.000 | 1.000 |
| 4  | Numbers of iterations and fix rate of UWL FCB | 3 | 1.000 | 1.000 |
| 5  | Numbers of iterations and fix rate of UWL FCB | 3 | 1.000 | 1.000 |
| 6  | Numbers of iterations and fix rate of UWL FCB | 3 | 0.994 | 0.994 |
| 7  | Numbers of iterations and fix rate of UWL FCB | 2 | 1.000 | 1.000 |
| 8  | Numbers of iterations and fix rate of UWL FCB | 2 | 1.000 | 1.000 |
| 9  | Numbers of iterations and fix rate of UWL FCB | 2 | 1.000 | 1.000 |
| 10 | Numbers of iterations and fix rate of UWL FCB | 2 | 1.000 | 1.000 |
| 11 | Numbers of iterations and fix rate of UWL FCB | 2 | 1.000 | 1.000 |
| 12 | Numbers of iterations and fix rate of UWL FCB | 2 | 1.000 | 1.000 |

**Fig. 12** FCB estimation process document for ultra-wide lane

|                         |  |   |       |       |
|-------------------------|--|---|-------|-------|
| upd_debug_w_2023038.txt |  |   |       |       |
| 1                       | Numbers of iterations and fix rate of WL FCB | 3 | 1.000 | 0.998 |
| 2                       | Numbers of iterations and fix rate of WL FCB | 3 | 0.996 | 0.988 |
| 3                       | Numbers of iterations and fix rate of WL FCB | 3 | 0.981 | 0.972 |
| 4                       | Numbers of iterations and fix rate of WL FCB | 2 | 0.995 | 0.988 |
| 5                       | Numbers of iterations and fix rate of WL FCB | 3 | 0.992 | 0.984 |
| 6                       | Numbers of iterations and fix rate of WL FCB | 3 | 0.998 | 0.992 |
| 7                       | Numbers of iterations and fix rate of WL FCB | 3 | 0.998 | 0.990 |
| 8                       | Numbers of iterations and fix rate of WL FCB | 3 | 0.998 | 0.991 |
| 9                       | Numbers of iterations and fix rate of WL FCB | 2 | 0.999 | 0.991 |
| 10                      | Numbers of iterations and fix rate of WL FCB | 3 | 0.999 | 0.994 |
| 11                      | Numbers of iterations and fix rate of WL FCB | 2 | 0.990 | 0.987 |
| 12                      | Numbers of iterations and fix rate of WL FCB | 3 | 0.999 | 0.996 |

**Fig. 13** FCB estimation process document for wide lane

|                         |  |   |       |       |
|-------------------------|--|---|-------|-------|
| upd_debug_n_2023038.txt |  |   |       |       |
| 21                      | Numbers of iterations and fix rate of NL FCB | 5 | 0.960 | 0.884 |
| 22                      | Numbers of iterations and fix rate of NL FCB | 3 | 0.968 | 0.895 |
| 23                      | Numbers of iterations and fix rate of NL FCB | 3 | 0.965 | 0.905 |
| 24                      | Numbers of iterations and fix rate of NL FCB | 3 | 0.971 | 0.909 |
| 25                      | Numbers of iterations and fix rate of NL FCB | 2 | 0.984 | 0.927 |
| 26                      | Numbers of iterations and fix rate of NL FCB | 3 | 0.983 | 0.925 |
| 27                      | Numbers of iterations and fix rate of NL FCB | 3 | 0.974 | 0.929 |
| 28                      | Numbers of iterations and fix rate of NL FCB | 2 | 0.982 | 0.931 |
| 29                      | Numbers of iterations and fix rate of NL FCB | 3 | 0.969 | 0.917 |
| 30                      | Numbers of iterations and fix rate of NL FCB | 3 | 0.974 | 0.913 |
| 31                      | Numbers of iterations and fix rate of NL FCB | 5 | 0.966 | 0.909 |
| 32                      | Numbers of iterations and fix rate of NL FCB | 3 | 0.979 | 0.917 |
| 33                      | Numbers of iterations and fix rate of NL FCB | 3 | 0.978 | 0.922 |
| 34                      | Numbers of iterations and fix rate of NL FCB | 3 | 0.980 | 0.936 |
| 35                      | Numbers of iterations and fix rate of NL FCB | 3 | 0.979 | 0.935 |
| 36                      | Numbers of iterations and fix rate of NL FCB | 3 | 0.980 | 0.950 |
| 37                      | Numbers of iterations and fix rate of NL FCB | 3 | 0.982 | 0.940 |
| 38                      | Numbers of iterations and fix rate of NL FCB | 3 | 0.971 | 0.934 |
| 39                      | Numbers of iterations and fix rate of NL FCB | 3 | 0.976 | 0.944 |
| 40                      | Numbers of iterations and fix rate of NL FCB | 3 | 0.982 | 0.947 |
| 41                      | Numbers of iterations and fix rate of NL FCB | 3 | 0.974 | 0.950 |
| 42                      | Numbers of iterations and fix rate of NL FCB | 4 | 0.991 | 0.965 |
| 43                      | Numbers of iterations and fix rate of NL FCB | 4 | 0.994 | 0.976 |
| 44                      | Numbers of iterations and fix rate of NL FCB | 6 | 0.997 | 0.978 |
| 45                      | Numbers of iterations and fix rate of NL FCB | 3 | 0.998 | 0.995 |
| 46                      | Numbers of iterations and fix rate of NL FCB | 3 | 0.998 | 0.989 |
| 47                      | Numbers of iterations and fix rate of NL FCB | 3 | 1.000 | 0.998 |
| 48                      | Numbers of iterations and fix rate of NL FCB | 4 | 0.990 | 0.988 |

**Fig. 14** FCB estimation process document for narrow lane

**(3) Code:** The directory contains the program for estimating FCB, and the main program in it is “main.m” script. Implement FCB estimation by executing this program to call other programs. The input data includes satellite altitude angle files, raw frequency float ambiguity files, and cycle slip files.

**(4) Tools:** In order to facilitate users in calculating the input files required for the operation of the M\_FCB software. We provide a tool for computer input files. This program was developed again

based on the open-source software GAMP developed by Zhou et al. (2018), and is used the same way as GAMP software, both of which execute the program by reading control files. For detailed operation methods, please refer to "readme.docx" in this directory.

**(5) Example:** In the M\_FCB software, we provide a calculation example in the directory "data/2023038\_E/", which includes three types of input files. The running results can be compared with the results in the "result" directory, such as "result\_E\_2023038\_example". Users only need to configure the input file directory, solution control file, and output result directory correctly.

## 4. How to Run the Software

### 4.1 MATLAB version

Although the M\_FCB software is developed based on the MATLAB 2016a, the algorithms and functions used in the software are almost all developed by us. Therefore, the debugging and use of M\_FCB softer supports almost all MATLAB versions.

### 4.2 M\_FCB software operation method

The user needs to open the directory of the "main.m" script in the MATLAB interface, and then realize the FCB estimation by setting the control parameters and run the "main.m" script. That means the M\_FCB software starts by running the "main.m" function. During the FCB estimation process, the "main.m" function will sequentially call other sub functions until the FCB solution is completed. Several important points are explained as follows:

**(1) Solution time setting.** Before running the "main.m" function, users need to set the solution time (as shown in the green box in Figure 15). Because this time is also the time in the FCB output file. The time format is a year with four characters and day of year (DOY) with three characters.

**(2) Input data path settings.** The input path here mainly refers to the path of the input files, as shown in the red box in Figure 15. After configuring the path, the program will automatically read the raw frequency float ambiguity file, satellite elevation angle file, and cycle slip file from the path.

**(3) Solution system selection.** The M\_FCB software is a single system solution. It divides BDS-2 and BDS-3 into two systems. Users can determine which satellite system to solve by setting the value of "NavSystem".

**(4) Output path settings.** The output path here mainly refers to the output path of FCB solution results and their corresponding process files. In general, the default output path is in the code directory. Users can set the output path from 'UD\_dead\_configured.m'. As shown in the red box in Figure 15.

**(5) Run "main.m".** After all configuration information is completed, users can run the main function file to implement FCB estimation.



```

main.m
1  clc;
2  clear;
3  format long
4  %% FCB/UPD estimation softer
5  % FCB/UPD estimation on both raw frequency and combined frequency
6  % Default system: GPS(G), Galileo(E), BDS-2(C2) and BDS-3(C3)
7  % Default frequency: G(L1 L2 L3), E(E1 E5a E5b), C2/3(B1I B3I B2I/B2a)
8  % made by Caiya Yue @ China University of Mining & Technology,Beijing (CUMTB)
9  %                               @ Chinese Academy of Surveying and Mapping (CASM)
10 %                               @ Liaocheng University (LCU)
11 % -----
12 %
13 %% Common parameter settings
14 data_dir='E:\data\data for paper FCB\2023038\result E 20240705\';
15 yyyy=2023;
16 doy=038;
17 NavSystem=2; % 1:GPS 2:Galileo (GAL) 3:BDS-2 (BD2) 4:BDS-3 (BD3)

```

Fig. 15 Important setting options in the main function

```

UD_read_configuration.m
52 if(cfg.NavSystem==4); cfg.NPRN=60; end
53 if(cfg.NavSystem==4)
54     cfg.new_ban=2; % 1:B1C 2:B2a
55 end
56 %-----Arc segment merging control strategy-----
57 if(cfg.NavSystem==1); cfg.comb_time=90; end % minimum arc segment for merging (min)
58 if(cfg.NavSystem==2); cfg.comb_time=120; end
59 if(cfg.NavSystem==3); cfg.comb_time=120; end
60 if(cfg.NavSystem==4); cfg.comb_time=120; end
61 %-----Excluded satellites-----
62 if(cfg.NavSystem==1); cfg.rem_prn='00 00'; end
63 if(cfg.NavSystem==2); cfg.rem_prn='00 12 13 15 19 24 25'; end
64 if(cfg.NavSystem==3); cfg.rem_prn='00 00'; end
65 if(cfg.NavSystem==4); cfg.rem_prn='00 36 41 42'; end
66 cfg.comb_arc=30; % merge the data from the last 30 minutes as the ambiguity parameter
67 cfg.nprn_C2=16; % number of BDS-2 satellites
68 cfg.geo_flag=0; % 0: do not estimate GEO satellite; 1:estimate GEO satellite
69 cfg.ref_prn=0; % 0: max satellite 1: max site
70 %-----Output section settings-----
71 if(cfg.doy<100 && cfg.doy>9); s_doy=strcat('0',num2str(cfg.doy)); end
72 if(cfg.doy<10); s_doy=strcat('00',num2str(cfg.doy)); end
73 if(cfg.doy>99); s_doy=num2str(cfg.doy); end
74 if(cfg.NavSystem==1); out_dir=strcat('result_G_',num2str(cfg.yyyy),s_doy); end
75 if(cfg.NavSystem==2); out_dir=strcat('result_E_',num2str(cfg.yyyy),s_doy); end
76 if(cfg.NavSystem==3); out_dir=strcat('result_C2_',num2str(cfg.yyyy),s_doy); end
77 if(cfg.NavSystem==4); out_dir=strcat('result_C3_',num2str(cfg.yyyy),s_doy); end
78 cfg.out_dir=out_dir;
79 end

```

Fig. 16 Important setting options in the configuration script

### 4.3 How to set whether the input file is read

If the user is debugging or solving the FCB on the same day, it obviously takes some time to read the input file repeatedly. Therefore, we stored the read FCB data in file “\*.mat” file (as shown in the Figure 13). If the user performs another debugging and reconciliation on the same day and does not change the input data, it can avoid spending a certain amount of time to read the input file again. Of course, if the user's input data changes, you need to read them again. Users only need to delete these “\*.mat” files under the result directory.

| 名称  | 修改日期           | 类型     | 大小        |
|---|----------------|--------|-----------|
| <input type="checkbox"/> Aelev12.mat            | 2024/7/25 7:54 | MAT 文件 | 53 KB     |
| <input type="checkbox"/> Aelev23.mat            | 2024/7/25 7:54 | MAT 文件 | 53 KB     |
| <input type="checkbox"/> Aelev43.mat            | 2024/7/25 7:54 | MAT 文件 | 53 KB     |
| <input type="checkbox"/> Arra_amb1_2023038.mat  | 2024/7/25 7:44 | MAT 文件 | 4,705 KB  |
| <input type="checkbox"/> Arra_amb2_2023038.mat  | 2024/7/25 7:44 | MAT 文件 | 5,264 KB  |
| <input type="checkbox"/> Arra_amb3_2023038.mat  | 2024/7/25 7:45 | MAT 文件 | 5,219 KB  |
| <input type="checkbox"/> Arra_cslip_2023038.mat | 2024/7/25 7:50 | MAT 文件 | 784 KB    |
| <input type="checkbox"/> Arra_elev_2023038.mat  | 2024/7/25 7:49 | MAT 文件 | 10,271 KB |
| <input type="checkbox"/> cgs2023038_LC_E.fcb    | 2024/7/25 7:57 | FCB 文件 | 100 KB    |
| <input checked="" type="checkbox"/> figure4.png | 2024/7/25 7:57 | PNG 文件 | 35 KB     |
| <input checked="" type="checkbox"/> figure5.png | 2024/7/25 7:57 | PNG 文件 | 41 KB     |
| <input checked="" type="checkbox"/> figure6.png | 2024/7/25 7:57 | PNG 文件 | 41 KB     |
| <input type="checkbox"/> FTamb12.mat            | 2024/7/25 7:54 | MAT 文件 | 57 KB     |
| <input type="checkbox"/> FTamb23.mat            | 2024/7/25 7:54 | MAT 文件 | 59 KB     |
| <input type="checkbox"/> FTamb43.mat            | 2024/7/25 7:54 | MAT 文件 | 60 KB     |
| <input type="checkbox"/> noexist_amb1_sta.txt   | 2024/7/25 7:33 | 文本文件   | 0 KB      |
| <input type="checkbox"/> noexist_amb2_sta.txt   | 2024/7/25 7:36 | 文本文件   | 0 KB      |
| <input type="checkbox"/> noexist_amb3_sta.txt   | 2024/7/25 7:40 | 文本文件   | 0 KB      |
| <input type="checkbox"/> noexist_cslip_sta.txt  | 2024/7/25 7:49 | 文本文件   | 0 KB      |
| <input type="checkbox"/> noexist_elev_sta.txt   | 2024/7/25 7:45 | 文本文件   | 0 KB      |
| <input type="checkbox"/> Read_amb1_2023038.mat  | 2024/7/25 7:36 | MAT 文件 | 5,906 KB  |
| <input type="checkbox"/> Read_amb2_2023038.mat  | 2024/7/25 7:40 | MAT 文件 | 6,622 KB  |
| <input type="checkbox"/> Read_amb3_2023038.mat  | 2024/7/25 7:43 | MAT 文件 | 6,565 KB  |
| <input type="checkbox"/> Read_cslip_2023038.mat | 2024/7/25 7:50 | MAT 文件 | 758 KB    |
| <input type="checkbox"/> Read_elev_2023038.mat  | 2024/7/25 7:48 | MAT 文件 | 13,096 KB |

Fig. 17 Several “\*.mat” files under the result directory.

## 5. Availability analysis of FCB

A total of globally and uniformly distributed 180 multi-GNSS experiment (MGEX) stations (Figure 18) were selected to implement GPS, Galileo, BDS-2 and BDS-3 satellite FCB estimation. The time range was DOY 038~051 in 2023. All the stations can receive triple-frequency observation data with a sampling rate of 30 s. In order to verify the usability of the FCB product, 24 stations (Figure 18) were selected for AR. The precision ephemeris was adopted from the final product released by the international GNSS service (IGS) analysis center of Wuhan university. The PCO/PCV at the satellite and receiver ends were corrected using the "igs20.atx" file released by IGS.

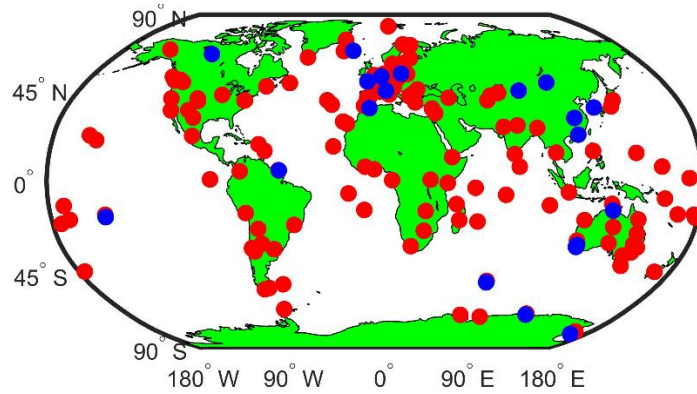


Fig. 18 Distribution of the FCB estimation and test stations

### 5.1 UWL-WL-NL FCB

Different from existing research, Figure 19 takes the Galileo satellite system as an example to show the FCB time series of UWL, WL, and NL with a time resolution of 30 minutes in a single day. Overall, UWL FCB has better stability than WL FCB, and WL FCB has better stability than NL FCB. Analysis shows that the UWL and WL FCB of the satellite have very high single day stability, and can be estimated to implement ambiguity fixation continuously within a single day. Statistics



show that the STD of UWL FCB and WL FCB are 0.0034 and 0.028 weeks, respectively.

The NL FCB series exhibited more significant fluctuations compared with the UWL FCB and WL FCB. This is mainly because the precision of satellite precise products, the effect of pseudo-range code bias correction and the number of observable satellites can affect the stability of the FCB estimation to a certain extent. Further analysis reveals that the STD of Galileo NL FCB is about 0.035 cycles. In  $M\_FCB$ , the NL FCB was obtained from the raw float-ambiguity ionosphere-free combinations. The ionosphere-free combinations had short wavelengths and thus were susceptible to the effects of adjustment models and observation errors. Consequently, the ionosphere-free combinations were difficult to maintain stability over long periods. A set of NL FCBs needs to be estimated at regular intervals. It is worth noting that, for the FCBs with better one-day stability, a single value of one-day estimation can be achieved by taking the average of all FCBs in a day. For the FCBs with lower one-day stability, the control file can be used to set the interval length.

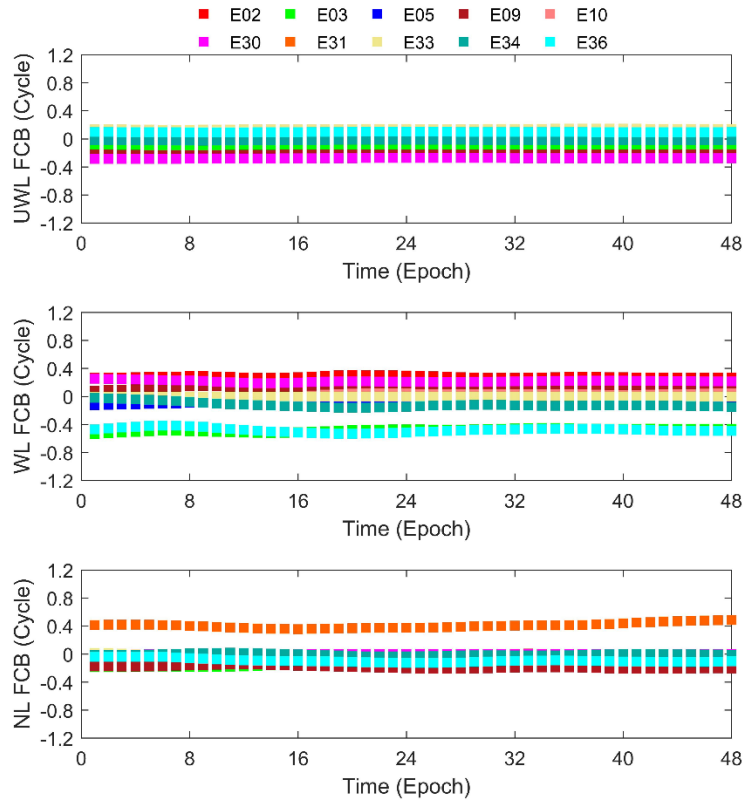


**Fig. 19** FCB time series of UWL, WL, and NL within a single day

## 5.2 Raw frequency FCB

Figure 20 shows the raw frequency FCB of some satellites using the Galileo satellite system as an example. Analysis shows that the FCB at each raw frequency exhibits significant time-varying characteristics and large fluctuations. Statistics show that the STD of FCB on the first, second, and third frequencies are approximately 0.14, 0.12, and 0.07 cycles, respectively. The stability is significantly lower than the FCB of the combined satellite. In addition, the time-varying nature of FCB at the raw frequency is complex, which is not conducive to modeling, forecasting, and single day estimation. Therefore, the traditional method is to convert the original frequency FCB into a

linear combination of FCBs based on the design matrix.

The linear combination of FCB time series is shown in Figure 21. Among them, the ultra wide lane FCB combination is (0 1 -1), the wide lane linear combination is (1-1 0), and the narrow lane linear combination is (4-3 0). Analysis shows that the linear combination of FCB time series changes very steadily, which is basically consistent with the time-varying characteristics of UWL-WL-NL FCB sequence. Statistics show that the STD values of UWL, WL, and NL FCB obtained by this method are 0.0035, 0.040, and 0.044 cycles, respectively. The stability of WL and NL FCB is not as good as the results obtained by the UWL-WL-NL FCB estimation method. The main reason may be that the NL ambiguity is easily affected by ionospheric delay bias and other unmodeled biases, resulting in lower accuracy. When the mandatory inclusion of UWL, WL, and NL float ambiguities into a system of equations affects the WL FCB estimation results. However, due to the relatively longer wavelength of UWL, it is basically unaffected. Undeniably, the significant advantage of the original frequency FCB estimation method is that users can freely combine FCBs to meet their needs.

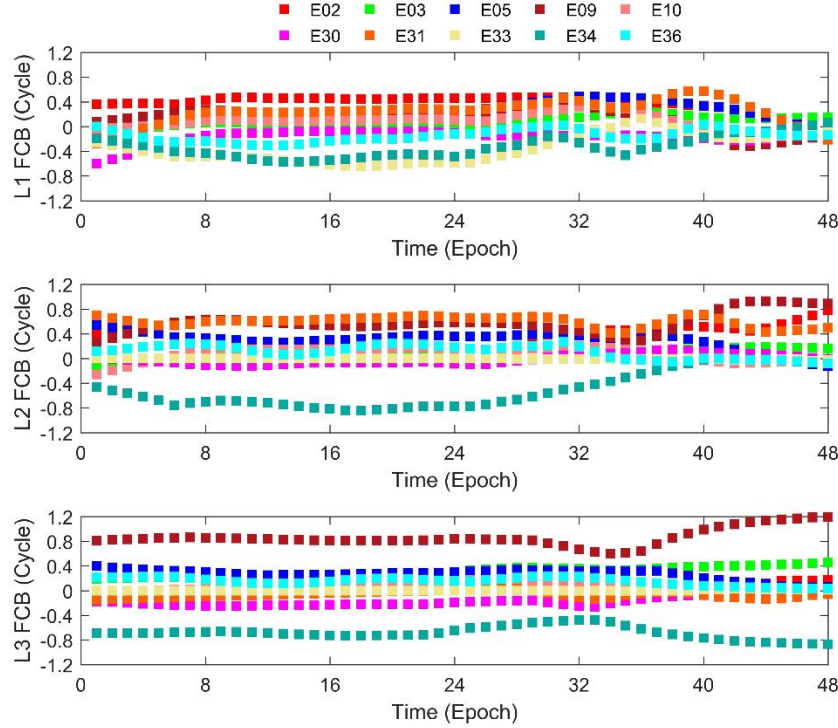


**Fig. 20** FCB time series of raw frequency within a single day

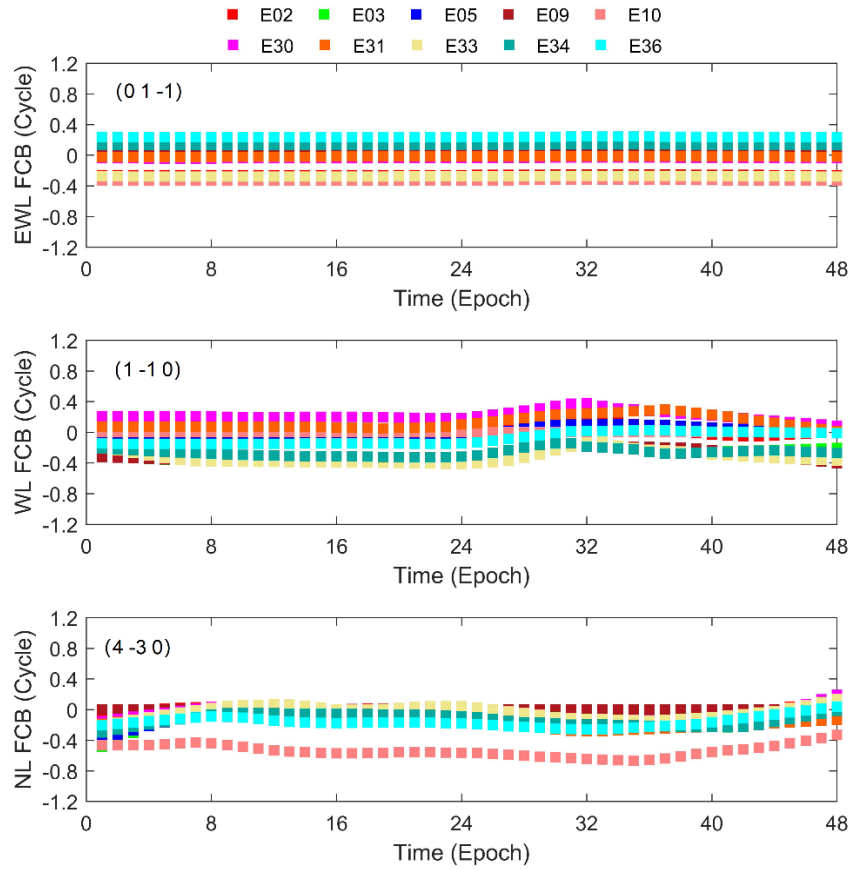


**Fig. 21** Time series of UWL, WL and NL combination FCB within a single day

### 5.3 Validations of PPP AR with FCB correction

In order to verify the availability of FCB calculated by  $M\_FCB$ , we implemented static and dynamic PPP ambiguity fixed solutions for 24 evenly distributed measurement stations worldwide. There are three schemes to compare the advantages of multi-system fusion float solution and ambiguity fixed solution. The three schemes are single GPS system float solution, GPS/Galileo/BDS fusion float solution, and GPS/Galileo/BDS fusion fixed ambiguity solution. The static PPP residual sequences of three schemes are shown in Figure 22.

Analysis shows that regardless of whether it is a float solution or a fixed solution, the positioning accuracy of multi-system combined PPP is better than that of a single system, indicating that the increase in the number of satellites has improved the geometric configuration of satellite positioning and enhanced the strength of the adjustment system, thereby improving the positioning accuracy. Compared to float solutions, fixed solutions can significantly improve the performance of three-dimensional directional positioning, especially in the east direction, which is most obvious and can achieve a level of accuracy consistent with the north direction component. Statistics show that after fixing the ambiguity, the positioning accuracy in the horizontal and vertical directions can be improved by 20.34% and 21.76%, respectively.

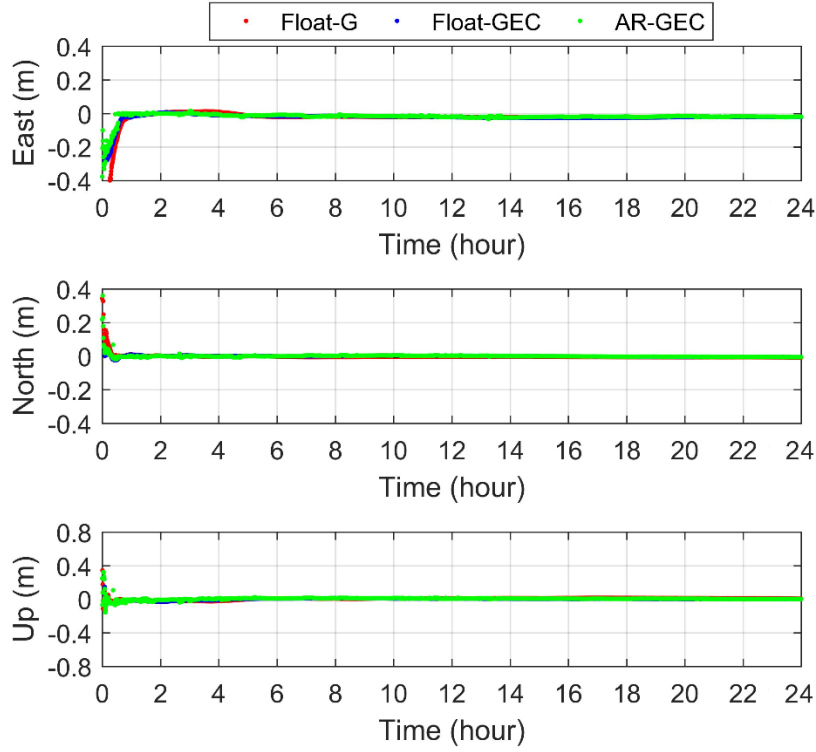


**Fig. 22** Triple-frequency uncombined static PPP coordinate residual series at KRGG station

Kinematic positioning is an effective method for assessing the performance of PPP AR. Therefore, we conducted a simulated kinematic PPP ambiguity fixed analysis on these 24 MGEX testing stations. The station coordinates were estimated through random walk in the solution. In order to be consistent with the FCB estimated in this paper, the precise orbit and clock bias products released by the WHU analysis center were used. The other parameter corrections (e.g., PCO, PCV and DCB) were strictly consistent with the corrections used in the FCB estimation. Station coordinate references were available from the IGS weekly solution.

The time series of coordinate residuals of the float and fixed solutions of the ambiguity in the east, north and vertical directions are given as an example for the KRGG station (Figure 23). In order to eliminate the effect of large fluctuations of coordinate residuals in the convergence stage of ambiguity, the root mean square (RMS) of coordinate residuals was counted after the convergence was stabilized (about 1 h). Comparing the GPS single-system float solution and the GPS/Galileo/BDS-2/BDS-3 (GEC) multi-system float solution, it is known that integrated positioning of multi-satellite systems can improve the positioning performance of the coordinate solution. The average RMS values in horizontal and vertical directions can be reduced by 32.4% and 28.3%, respectively. By comparing the Float-GEC and AR-GEC, the ambiguity-fixed kinematic PPP solution was significantly improved in terms of three-dimensional coordinate accuracy and positioning stability relative to the float solution. The average RMS values of the fixed coordinate residuals in the east, north and vertical directions for all test stations were reduced by 30.3%, 12.5% and 16.0%, respectively. Figure 23 also shows that the convergence of the coordinate residuals was accelerated after AR in these three directions (Particularly in the east and vertical directions). Therefore, the AR method using FCB correction is an effective means to improve the kinematic PPP performance.

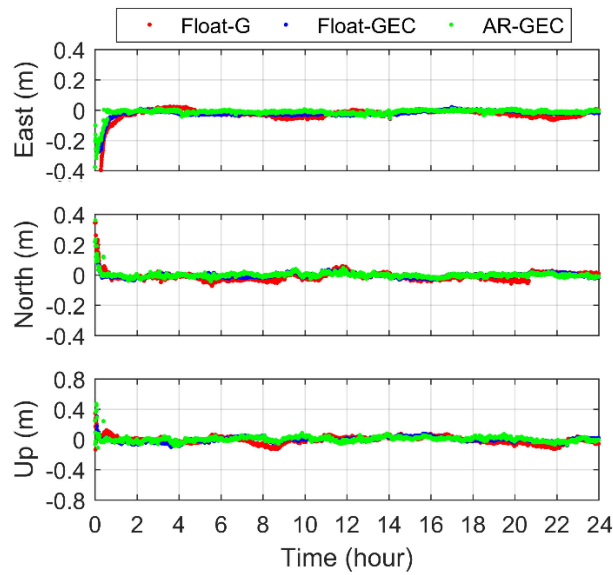


**Fig. 23** Triple-frequency uncombined kinematic PPP coordinate residual series at KRGG station

## 6. Acknowledgement and support

This software is developed based on MATLAB R2016a, and we are grateful to developers for their works. We would like to thank the IGS, CODE, CAS, IGN, etc. for providing GNSS observations and products. Most of the data used in the experiments can be downloaded from the IGS data center. We are grateful to Zhou et al. (2018) for their early work, because the input data of M\_FCB is calculated based on GAMP secondary development.

## 7. References

- Hatch R (1982) The synergism of GPS code and carrier measurements. In: Proceedings of the third international symposium on satellite Doppler positioning at physical sciences laboratory of New Mexico State University. 2 (8): 1213–1231
- Li X, Han X, Li X, Liu G, Feng G, Wang B, Zheng H (2021) GREAT-UPD: An open-source software for uncalibrated phase delay estimation based on multi-GNSS and multi-frequency observations. *GPS Solut* 25, 66 (2021). <https://doi.org/10.1007/s10291-020-01070-2>
- Li P, Zhang Xi, Ge M, Schuh H (2018) Three-frequency bds precise point positioning ambiguity resolution based on raw observables. *Journal of Geodesy*, 92(12), 1357–1369.
- Melbourne WG (1985) The case for ranging in GPS-based geodetic systems. In: Proceedings of the first international symposium on precise positioning with the global positioning system, Rockville, US, pp 373–386
- Wübbena G (1985) Software developments for geodetic positioning with GPS using TI-4100 code and carrier measurements. In: Proceedings of the first international symposium on precise positioning with the global positioning system, Rockville, US, pp 403–412

Zhou F, Dong D, Li W, Jiang X, Wickert J (2018) GAMP: An open-source software of multi-GNSS precise point positioning using undifferenced and uncombined observations. *GPS Solut* doi.org/10.1007/s10291-018-0699-9.